[13]. Consistent with these results, *Mgmt*$^{-/-}$ *Mlh1*$^{-/-}$ cells, derived from the gene-targeted mice, are unable to induce apoptosis and show an elevated mutant frequency after MNU treatment [14].

The apoptotic signal initiated through the mismatch recognition complex activates a signaling cascade leading to the cell cycle checkpoints and apoptotic pathways for cell death. Both the release of cytochrome C from the mitochondria as well as the activation of Apaf-1 and caspase-3, hallmarks of the induction of apoptosis, have been demonstrated after the treatment of cells with alkylating agents that produce O^6-methylguanine [14,15]. However, the precise molecular mechanism underlying the signal transduction downstream of mismatch recognition still remains to be determined. To identify the factors involved in the O^6-methylguanine-induced apoptotic process, we screened MNU-resistant clones derived from MNU-sensitive *Mgmt*$^{-/-}$ cells using retrovirus-mediated gene-trap mutagenesis [16]. Mouse-derived KH101 cells, carrying an insertional mutation in one of the alleles of an uncharacterized gene, were unable to induce mitochondrial membrane depolarization as well as caspase-3 activation, after treatment with MNU. In this way, we identified a new gene, designated as *Mapo1* (O^6-methylguanine induced apoptosis 1), which was related to the induction of apoptosis. The mutant frequency of KH101 cells was significantly elevated after the treatment with MNU, thus supporting the notion that the induction of apoptosis, in which the MAPO1 is involved, contributes significantly to the elimination of cells carrying mutation-inducing DNA lesions. A search in the database revealed that the amino acid sequence of the MAPO1 protein is homologous to that of folliculin-interacting protein 1 (FNIP1), which was identified as a protein having the capacity to associate with folliculin [17]. Folliculin is a tumor suppressor protein with unknown biological activity, and is encoded by the *FLCN* gene. Mutations in the *FLCN* gene have been found in patients with Birt-Hogg-Dubé (BHD) syndrome [18,19], which is characterized by the development of hair follicle hamartomas, lung cysts, and an increased risk for renal neoplasia [20–22]. Identification of another folliculin-interacting protein, displaying a similarity in its amino acid sequence to that of FNIP1, was reported by two groups of researchers and the gene responsible was named *FNIP2* and *FNIPL*, respectively [23,24]. The *FNIP2/FNIPL* gene turned out to be the same gene as the human homolog of *Mapo1*. It was also reported that FNIP2/FNIPL, as well as FNIP1, could bind to 5′-AMP-activated protein kinase (AMPK), composed of AMPKα, β and γ subunits, which is an important energy sensor in cells that negatively regulates cell growth and proliferation [25,26].

We report here that a complex composed of MAPO1, FLCN and AMPK is involved in the induction of apoptosis triggered by O^6-methylguanine–thymine mispair. Evidence is presented which shows that during the course of apoptosis induction, the phosphorylation of AMPKα occurs in a MAPO1- and FLCN-dependent manner.

2. Materials and methods

2.1. Cell lines and cell culture

The YT102 (*Mgmt*$^{-/-}$ *Mlh1*$^{+/+}$), YT103 (*Mgmt*$^{-/-}$ *Mlh1*$^{-/-}$) and KH101 (*Mgmt*$^{-/-}$ *Mapo1*$^{+/-}$) cell lines were established as described previously [14,16]. The cells were cultivated in Dulbecco's modified Eagle's medium (D-MEM) supplemented with 10% fetal bovine serum (FBS) at 37 °C in 5% CO_2.

2.2. Chemicals

N-Methyl-*N*-nitrosourea (MNU) was obtained from Sigma. Compound C and AICA-Ribose were purchased from Calbiochem.

2.3. Immunoprecipitation and immunoblotting

To prepare cells expressing Flag-tagged MAPO1 or HA-tagged FLCN, a pIRES-puro3 vector (Clontech) containing mouse-derived *Mapo1* cDNA tagged with Flag epitope at the carboxy terminal end or a pIRES-puro2 (Clontech) vector carrying mouse-derived *Flcn* cDNA tagged with the HA epitope at the amino terminal end was introduced into YT102 cells using Lipofectamine 2000 (Invitrogen) according to the manufacturer's protocol. For the immunoprecipitation, the cells were lysed with NETN buffer (50 mM Tris/HCl (pH 8.0), 150 mM NaCl, 0.2% NP-40, 1 mM EDTA) containing protease inhibitors (Roche). To precipitate the Flag-tagged MAPO1, 10 μl of anti-FLAG M2-agarose (Sigma) were added to the extract, and incubated for 4 h at 4 °C. Alternatively, 10 μl of anti-HA (HA-7)-agarose (Sigma) were added to precipitate the HA-tagged FLCN, and the mixture was incubated overnight at 4 °C. After extensive washing of the beads with NETN buffer, the proteins bound to the beads were eluted in 40 μl of 2× SDS-PAGE sample buffer (120 mM Tris/HCl (pH 6.8), 4% SDS, 20% glycerol, 200 mM DTT, 0.002% bromophenol blue).

For the immunoblotting analyses, immunoprecipitated materials or whole cell extracts prepared by the lysis of cells with 2× SDS-PAGE sample buffer were subjected to SDS-PAGE and electroblotted onto a PVDF membrane (Bio-Rad). Detection was performed using an ECL Plus or Advance Western blotting detection kit (GE Healthcare). The primary antibodies used were: anti-FLAG M2 (Sigma), anti-HA HA-7 (Sigma), anti-FLCN (Protein Tech Group, Inc.), anti-AMPKα (Cell signaling), anti-β-actin (Sigma), and anti-phospho-AMPKα (Thr172) (Cell signaling). Anti-mouse IgG and anti-rabbit IgG conjugated to horseradish peroxidase (GE Healthcare) were used as the secondary antibodies.

2.4. siRNA transfection

Stealth RNAi for the *Mapo1* gene (siMapo1), 5′-CAGAAAGCAGAGGAUGUUCCUAUUA-3′, *Flcn* gene (siFlcn#1), 5′-UUAUUCAGGAUAGUGGGCCCAACUC-3′, (siFlcn#2), 5′-UGGUGACUGACGUACUUAAUAGAGG-3′, and *Ampkα* gene (siAmpkα#1), 5′-UAUCUUAGCGUUCAUCUGGGCAUCC-3′, (siAmpkα#2), 5′-AAGAUGAUAAGCCACUGCAAGCUGG-3′ were purchased from Invitrogen. After culturing 1×10^5 cells in a 6-well plate for one day, the cells were transfected with 20 nM siRNA, using the Lipofectamine RNAiMAX reagent (Invitrogen) according to the manufacturer's protocol. For the control transfection, Stealth RNAi Negative Control Medium GC Duplex (Invitrogen) was used.

2.5. Flow cytometric analysis

For the sub-G_1 population assay, cells were washed with PBS and suspended in 400 μl of PBS containing 0.1% Triton X-100, 25 μg/ml of propidium iodide and 0.1 mg/ml of RNase A. The samples were analyzed using a FACS Calibur flow cytometer (Becton Dickinson), with 10,000 events per determination.

For the mitochondrial membrane depolarization assay, cells were treated with the MitoProbeTM DiOC2(3) Assay Kit (Invitrogen), according to the manufacturer's protocol, and then subjected to analysis using a FACS Calibur flow cytometer.

2.6. Trypan blue exclusion assay

The viability of YT102, KH101 and siRNA-transfected YT102 cells was assayed, based on their trypan blue exclusion. The cells treated with AICA-Ribose were collected 48 h after the drug treatment and were stained with 0.2% trypan blue. The percentage of dead cells was determined as the percentage of trypan blue staining-positive cells. At least 500 cells were counted per experiment.

2.7. Statistics

All *P*-values were generated using two-tailed Student's *t*-tests.

3. Results

3.1. Interaction of MAPO1 with FLCN and AMPK

To confirm that MAPO1 protein interacts with FLCN and AMPK, a co-immunoprecipitation experiment was performed. Whole cell extracts were prepared from mouse YT102 (*Mgmt*$^{-/-}$) cells expressing Flag-tagged MAPO1, and were subjected to immunoprecipitation using an anti-Flag antibody conjugated to agarose beads. The results are shown in Fig. 1A. With whole cell extracts, almost the same intensity of bands for FLCN and AMPKα were detected in both control and Flag-MAPO1-transfected cells. When the materials were immunoprecipitated with the anti-Flag antibody, co-precipitated FLCN and AMPKα were clearly detected, concomitant with the effective precipitation of Flag-MAPO1, whereas no such bands were seen in a sample precipitated from cells treated with the control vector alone.

To evaluate the interaction of FLCN with MAPO1 and AMPK in a reciprocal manner, whole cell extracts prepared from YT102 cells expressing FLAG-tagged MAPO1, with or without HA-tagged FLCN, were applied for immunoprecipitation using an anti-HA antibody (Fig. 1B). When the HA-tagged FLCN was precipitated, as indicated by doublet bands by the immunoblotting analysis, the Flag-tagged MAPO1 and AMPKα were co-precipitated. It is evident, therefore, that MAPO1 interacts with FLCN and AMPK in mouse cells.

3.2. Suppression of the induction of apoptosis in Flcn- and Ampkα-knockdown cells

Since MAPO1 has been identified as an apoptosis-inducing protein, it is plausible that the MAPO1-bound proteins, FLCN and AMPK, might also be involved in apoptosis induction. To examine the possible roles of these proteins, siRNAs specific for the *Flcn* or *Ampkα* genes were introduced into YT102 (*Mgmt*$^{-/-}$) cells. As shown in Fig. 2A and B, two independent siRNAs (siFlcn#1 and #2, and siAmpkα#1 and #2), designed at different sequences of each gene, effectively suppressed the expression of the genes when measured at 48 h after their introduction. The expression level of the *Mapo1* gene in siMapo1-treated cells also decreased to 43% of that in cells that were treated with the control RNA, siCont, as measured by quantitative real time PCR [16]. To monitor the appearance of cells with sub-G_1 DNA content, cells were treated with or without 0.4 mM MNU for 1 h and subjected to a flow cytometric analysis 72 h later. After treatment with MNU, the sub-G_1 cell population increased to more than 20% in the siCont-treated cells (Fig. 2C). Under the same conditions, the degrees of the increases in the cells treated with siRNAs against the *Flcn*, *Ampkα* and *Mapo1* genes were significantly suppressed. These results favor the notion that FLCN and AMPKα, as well as MAPO1, are involved in MNU-induced apoptosis through protein interactions.

3.3. Suppression of the induction of apoptosis by an AMPK inhibitor

The effects of *Ampkα* knockdown on the MNU-induced apoptosis were further examined at multiple time points. The YT102 cells transfected with siCont or siAmpkα#2 were exposed to 0.4 mM MNU for 1 h and then subjected to a flow cytmetric analysis. As shown in Fig. 3A, the sub-G_1 cell population increased gradually, with similar kinetics in cells transfected with either type of siRNA, but the degree of the increase in cells transfected with siAmpkα was significantly lower than that of siCont-transfected cells.

To obtain further evidence supporting the involvement of AMPK in MNU-induced apoptosis, compound C, a specific inhibitor of AMPK, was used to downregulate the function of AMPK. YT102 cells were exposed to 0.4 mM MNU for 1 h, followed by incubation with or without 2 μM of compound C for 72 h, and then cells were subjected to a flow cytometric analysis. As shown in Fig. 3B, the sub-G_1 cell population in compound C-treated cells after MNU treatment significantly decreased in comparison to those not treated with the inhibitor. The inhibitory effects of compound C on AMPK activity were assessed by immunoblotting using an antibody that specifically recognizes a phosphorylated form of AMPKα, since AMPK is activated when the catalytic subunit of AMPKα becomes phosphorylated [27–29]. As shown in Fig. 3C, AMPK appeared to be activated after MNU treatment, while such activation was significantly suppressed by the exposure of cells to compound C. These findings are consistent with the notion that AMPK plays an important role in the induction of apoptosis triggered by MNU.

3.4. MAPO1- and FLCN-dependent activation of AMPK during the induction of apoptosis

To further examine if AMPKα is phosphorylated during the induction of apoptosis, YT102 cells were treated with 1 mM MNU and then collected at 0, 24, 48 and 72 h after treatment. Under these conditions, apoptosis was effectively induced, as was evident by the detection of the mitochondrial membrane depolarization and the caspase-3 activity [16]. The whole cell extracts were prepared, and the phosphorylation levels of AMPKα were assessed by

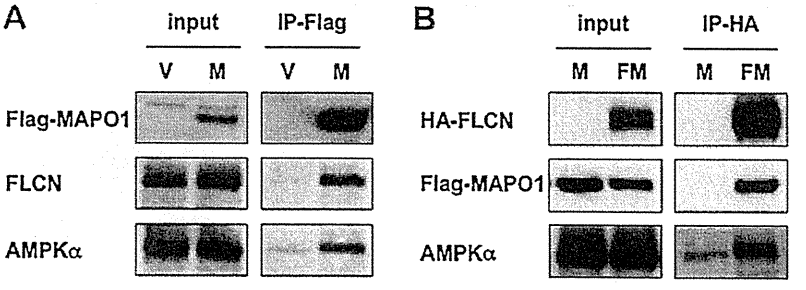

Fig. 1. The association of MAPO1, FLCN and AMPKα proteins. (A) The interaction of MAPO1 with FLCN and AMPKα. YT102 cells were transfected with the pIRES-puro3 vector (termed as V) or pIRES-puro3 containing Flag-tagged *Mapo1* cDNA (termed as M) and harvested after incubation for 24 h. Whole cell extracts (input) were used for immunoprecipitation using anti-Flag M2 antibody beads (IP-Flag). The materials were subjected to SDS-PAGE, transferred to a membrane and immunoblotted using antibodies that recognize the Flag-tag, FLCN and AMPKα. (B) The interaction of FLCN with MAPO1 and AMPKα. YT102 cells were transfected with either pIRES-puro3 containing Flag-tagged *Mapo1* cDNA (termed as M) or pIRE-puro2 carrying HA-tagged *Flcn* cDNA and pIRES-puro3 containing Flag-tagged *Mapo1* cDNA (termed as FM) and were harvested 24 h later. Following immunoprecipitation using anti-HA HA7 antibody beads (IP-HA), an immunoblotting analysis was performed as described in (A) with anti-HA, anti-Flag and anti-AMPKα antibodies.

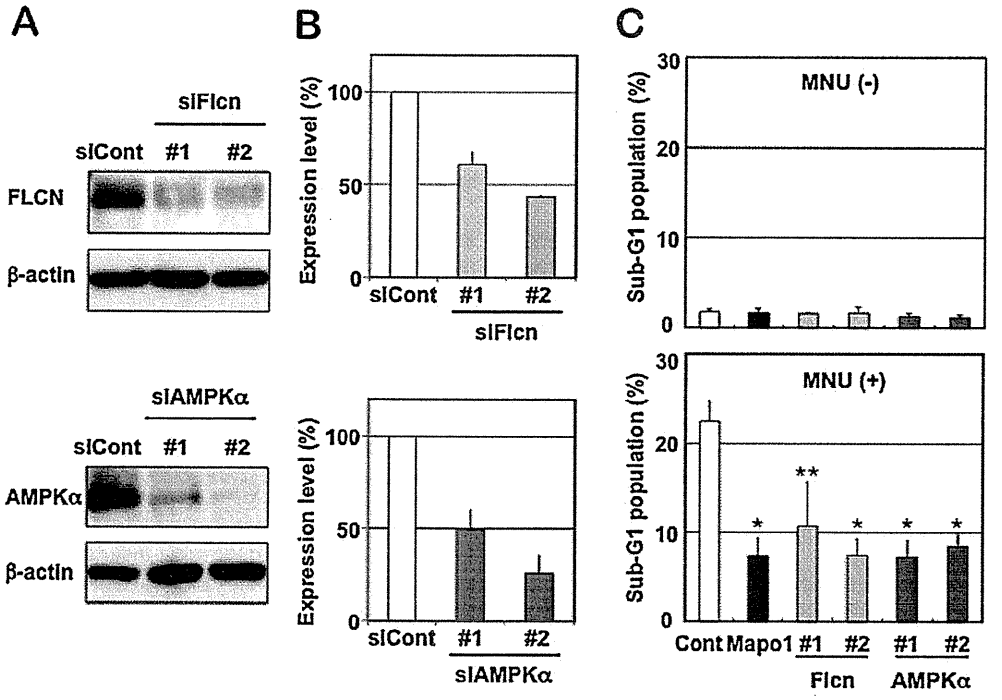

Fig. 2. The suppression of apoptosis by siRNAs targeting the three types of genes. (A) The expression levels of FLCN and AMPKα in cells treated with siRNAs. The whole extracts of YT102 cells transfected with control and two independent siRNAs specific for the corresponding genes were used for the immunoblotting analysis with antibodies specific for FLCN, AMPKα and β-actin (loading control). (B) The relative expression levels of FLCN and AMPKα in the cells treated with siRNAs, as measured by an immunoblotting analysis in (A). (C) The sub-G_1 population of cells transfected with control, *Mapo1*-, *Flcn*- or *Ampkα*-siRNA after MNU treatment. Two days after transfection with siRNA, YT102 cells were treated with or without 0.4 mM MNU for 1 h and then incubated for three days. The cells were harvested and subjected to a flow cytometric analysis. $^{*}P < 0.01$; $^{**}P < 0.05$ when comparing the sub-G_1 populations in the control and gene-specific siRNA-transfected cells.

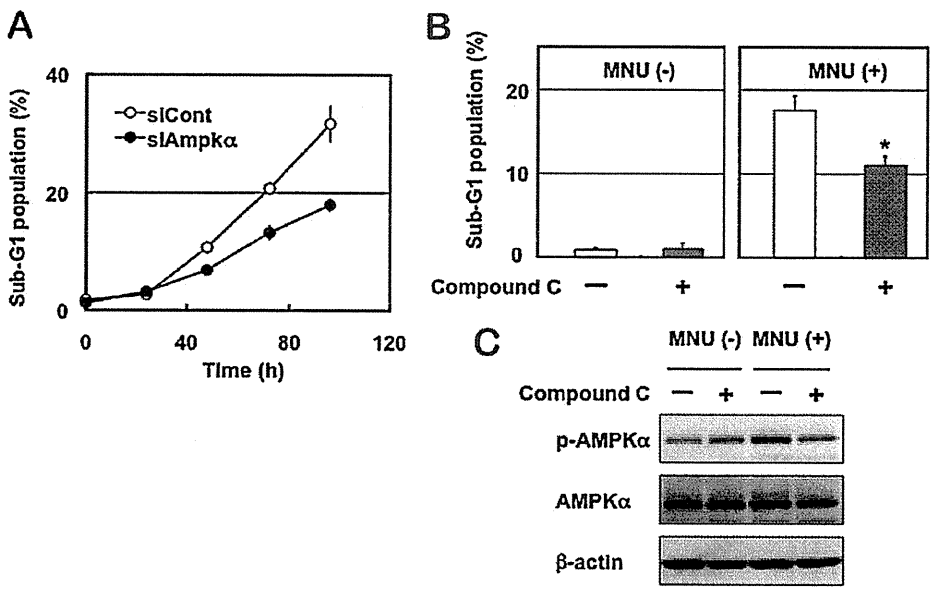

Fig. 3. The involvement of AMPK in MNU-induced apoptosis. (A) The sub-G_1 population of cells transfected with control or *Ampkα* siRNA after MNU treatment. Two days after transfection with siRNA, the YT102 cells were treated with 0.4 mM MNU for 1 h and then harvested at 0, 24, 48, 72 and 96 h after MNU treatment, and subjected to a flow cytometric analysis. The numbers of the cells in the sub-G_1 population were counted and the ratios were plotted. Open circles, siCont-transfected cells; closed circles, siAmpkα-transfected cells. (B) The suppression of apoptosis by an AMPK inhibitor. After treatment with or without 0.4 mM MNU for 1 h, YT102 cells were incubated in medium supplemented with or without 2 μM compound C for three days. The cells were then harvested and subjected to a flow cytometric analysis to monitor the sub-G_1 population of cells. $^{*}P < 0.01$ when comparing the sub-G_1 populations in compound C-untreated and compound C-treated cells after exposure to MNU. (C) The inhibition of the AMPK activity by compound C. The whole cell extracts from the cells harvested at 48 h after MNU treatment were subjected to an immunoblotting analysis using antibodies that recognize phospho-AMPKα (Thr172), AMPKα and β-actin, respectively.

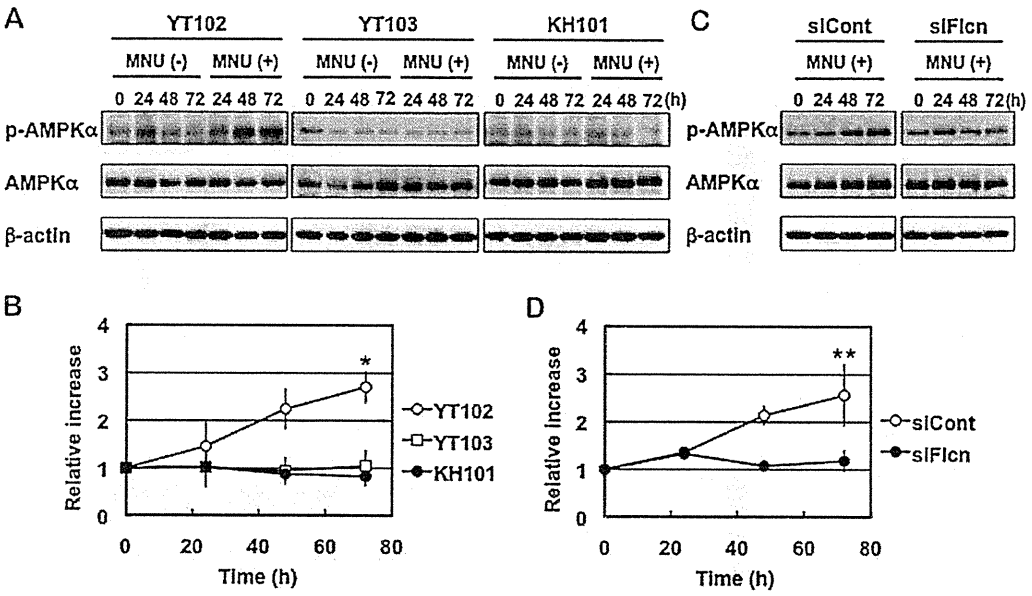

Fig. 4. The activation of AMPK after MNU treatment. (A) The phosphorylation of AMPKα in cells with different genetic backgrounds. Three cell lines, YT102 (*Mgmt*$^{-/-}$), YT103 (*Mgmt*$^{-/-}$ *Mlh1*$^{-/-}$) and KH101 (*Mgmt*$^{-/-}$ *Mapo1*$^{+/-}$), were treated with or without 1 mM MNU for 1 h and then incubated for 0, 24, 48 or 72 h. The whole cell extracts from cells harvested at various times after MNU treatment were subjected to an immunoblotting analysis using antibodies that recognize phospho-AMPKα (Thr172), AMPKα and β-actin, respectively. (B) The relative intensities of the bands for phospho-AMPKα (Thr172) after MNU treatment. Open circles, YT102; open squares, YT103; closed circles, KH101. *$P < 0.01$ when comparing the relative intensities for YT102 cells with those of the YT103 and KH101 cells at 72 h after exposure to MNU. (C) Activation of AMPK in cells transfected with *Flcn*-siRNA. Two days after transfection with control or *Flcn*-siRNA, the YT102 cells were treated with or without 1 mM MNU for 1 h. The analysis was performed as described above. (D) The relative intensities of bands for phospho-AMPKα (Thr172) after MNU treatment. Open circles, siCont-transfected cells; closed circles, siFlcn-transfected cells. **$P < 0.05$ when comparing the relative intensities of the control and *Flcn*-specific siRNA-transfected cells at 72 h after exposure to MNU.

an immunoblotting analysis. As shown in Fig. 4A and B, the levels of phosphorylation of AMPKα increased gradually and reached about 2.7-folds at 72 h after MNU treatment, whereas no such increase was observed in cells not expose to MNU. The amounts of the AMPKα protein were almost constant under these situations. In YT103 (*Mgmt*$^{-/-}$ *Mlh1*$^{-/-}$) cells, which are unable to induce apoptosis due to their lack of the *Mlh1* gene, the increase of phosphorylated forms of AMPKα was hardly detectable, even after MNU treatment. These results indicate that AMPK is activated during the course of the induction of apoptosis, triggered in a mismatch repair protein-dependent manner. To evaluate the effects of *Mapo1* mutation on the activation of AMPK, we used KH101 (*Mgmt*$^{-/-}$ *Mapo1*$^{+/-}$) cells, which carry an insertional mutation in one of the alleles of the *Mapo1* gene and exhibit haploinsufficiency for the induction of apoptosis triggered by MNU treatment [16]. Similar to the results described above, no increase in the band corresponding to phosphorylated AMPKα was detected even after treatment with MNU (Fig. 4A and B). Since MAPO1 interacts with FLCN (Fig. 1), it was supposed that FLCN might also play a role in the activation of AMPK during the course of apoptosis. To examine this possibility, YT102 (*Mgmt*$^{-/-}$) cells were transfected with siRNA targeting the *Flcn* gene (siFlcn#2), and then were exposed to 1 mM MNU for 1 h. The immunoblotting analyses of these samples collected after incubation for 0, 24, 48 and 72 h revealed that phosphorylation of AMPKα, which occurred gradually in siCont-transfected cells, did not take place in the siFlcn-transfected ones (Fig. 4C and D). These results indicate that the activation of AMPK, which occurs during the course of MNU-induced apoptosis, is dependent on the functions of both FLCN and MAPO1.

3.5. Induction of apoptosis through activation of AMPK

To confirm the importance of the activation of AMPK for the induction of apoptosis, AICA-Ribose (AICAR), a specific activator of AMPK, was applied to YT102 cells. After treatment with a low dose (0.2 mM) of AICAR for 48 h, the viabilities of cells were analyzed, based on the trypan blue exclusion assay. As shown in Fig. 5A, there was a significant increase of trypan blue staining-positive cells after treatment with AICAR in the YT102 (*Mgmt*$^{-/-}$ *Mapo1*$^{+/+}$) cells, whereas no such increase was observed in the *Mapo1*-defective KH101 (*Mgmt*$^{-/-}$ *Mapo1*$^{+/-}$) cells even after the same treatment. To determine if the increase in dead cells was related to the induction of apoptosis, the cells were subjected to an assay for mitochondrial membrane depolarization, which is known to occur during the process of apoptosis. The results are shown in Fig. 5B and C. The depolarization of the mitochondrial membrane was induced after treatment with AICAR in YT102 cells, but not in *Mapo1*-defective KH101 cells. The results indicate that the function of MAPO1 is necessary for AICAR-induced apoptosis. An immunoblotting experiment, the results of which are shown in Fig. 5D, revealed that the AICAR-treatment induced phosphorylation of AMPKα to the similar level to that when treated with MNU, however, such an induction did not occur in the *Mapo1*-defective KH101 cells. These results suggest that the activation of AMPK is important for the induction of apoptosis, and that a normal level of MAPO1 is necessary for the activation of AMPK.

We next examined if FLCN, which interacts with MAPO1, is also required for the AICAR-induced cell death. For this study, we applied AICAR to YT102 cells whose FLCN function was knocked down by siRNA (siFlcn#2). As shown in Fig. 6A–C, the degree of AICAR-induced cell death, which was accompanied by the depolarization of the mitochondrial membrane, was significantly lower in siFlcn-transfected cells as compared to that in siCont-transfected ones. Furthermore, the AICAR-induced AMPKα phosphorylation was almost completely blocked in siFlcn-transfected cells (Fig. 6D). Therefore, these results suggest that FLCN is required for AMPK activation, as well as the cell death induced by the treatment with AICAR.

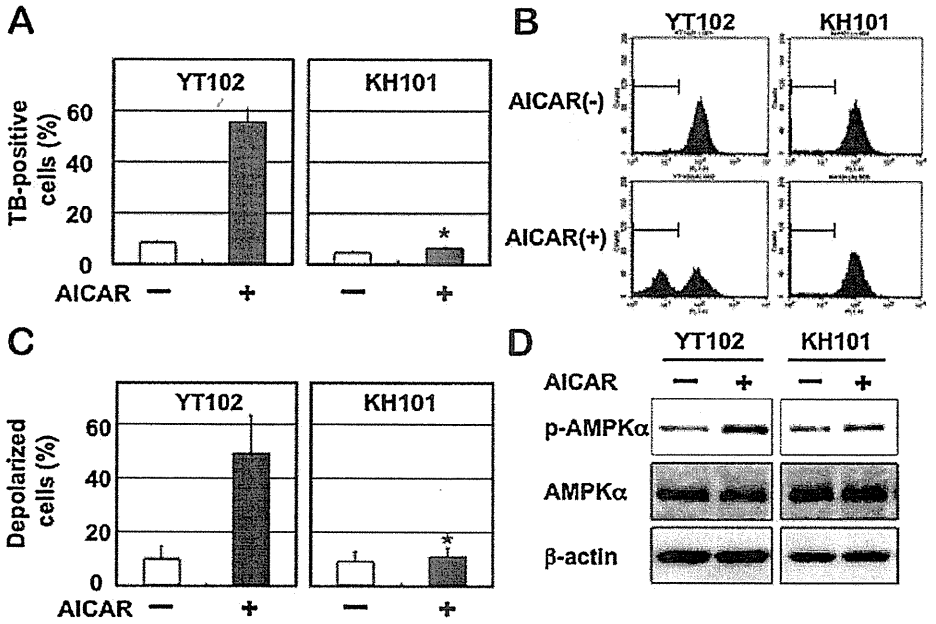

Fig. 5. MAPO1-dependent cell death induced by an AMPK activator. *Mapo1*-proficient YT102 and *Mapo1*-defective KH101 cells were incubated in a medium supplemented with or without 0.2 mM AICAR for two days and then harvested. (A) The viabilities of the cells. The numbers of cells stained with trypan blue (TB) were counted and the ratios are shown. $^*P < 0.01$ when comparing the TB-positive YT102 and KH101 cells after exposure to AICAR. (B) Depolarization of the mitochondrial membrane. The cells were evaluated by a mitochondrial membrane depolarization assay, and representative patterns of the assay are shown. The populations of depolarized cells were gated by bars. (C) The levels of mitochondrial membrane depolarization. The mean values obtained from three independent experiments in (B) and the standard deviations (bars) are presented. $^*P < 0.01$ when comparing the depolarized cells in YT102 and KH101 cells after exposure to AICAR. (D) Activation of AMPK after treatment with AICAR. The whole cell extracts prepared from cells, treated with or without AICAR, were subjected to an immunoblotting analysis using antibodies specific for phospho-AMPKα (Thr172), AMPKα and β-actin, respectively.

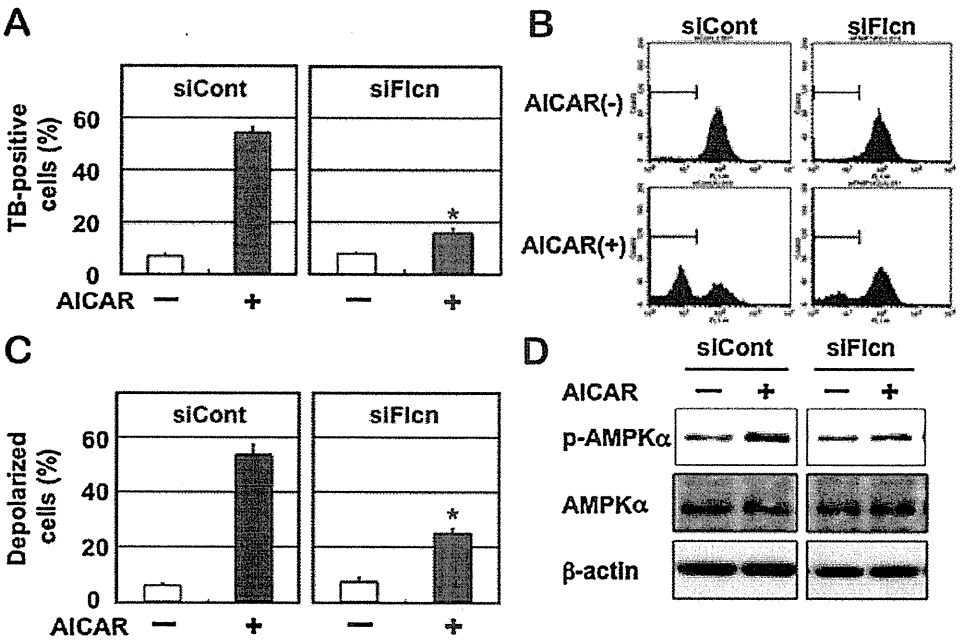

Fig. 6. FLCN-dependent cell death induced by an AMPK activator. YT102 cells transfected with control- or *Flcn*-siRNA were cultured with or without 0.2 mM AICAR for two days and then harvested. (A) The viabilities of the cells. The numbers of cells stained with trypan blue (TB) were counted and the ratios are shown. $^*P < 0.01$ when comparing the TB-positive siCont-transfected and siFlcn-transfected cells after exposure to AICAR. (B) Depolarization of the mitochondrial membrane. The cells were evaluated by a mitochondrial membrane depolarization assay, and representative patterns of the assay are shown. The populations of depolarized cells were gated by bars. (C) The levels of mitochondrial membrane depolarization. The mean values obtained from three independent experiments in (B) and the standard deviations (bars) are presented. $^*P < 0.01$ when comparing the depolarized cells in siCont-transfected and siFlcn-transfected cells after exposure to AICAR. (D) Activation of AMPK after treatment with AICAR. The whole cell extracts prepared from AICAR-treated or -untreated cells, were subjected to an immunoblotting analysis using antibodies specific for phospho-AMPKα (Thr172), AMPKα and β-actin, respectively.

4. Discussion

MAPO1 was identified as one of the protein elements functioning at a certain step following the induction of apoptosis [16]. In *Mapo1*-defective cells, mitochondrial membrane depolarization and caspase-3 activation were not observed even after exposure to MNU, although the cells retain the ability for mismatch repair protein-dependent DNA damage detection and signaling. Subsequent studies have revealed that MAPO1 is identical to FNIP2 and FNIPL, reported by Hasumi et al. [23] and Takagi et al. [24], respectively. This protein is bound to folliculin, encoded by the *FLCN* tumor suppressor gene, and AMP-activated protein kinase (AMPK). To analyze the possible roles of folliculin and AMPK in the induction of apoptosis, we introduced siRNAs specific for the *Flcn* or *Ampkα* gene and then treated the cells with MNU. The flow cytometric analyses performed to measure the sub-G_1 population of cells revealed that folliculin and AMPK, as well as MAPO1, were involved in MNU-induced apoptosis. Taken together, these data suggest that MAPO1 forms a protein complex(es) with folliculin and AMPK, and plays a role in a signal transduction pathway of apoptosis.

It is known that AMPK is one of the signaling kinases that negatively regulates cell growth and proliferation and is phosphorylated itself under conditions of energetic stress [26–29]. Several recent papers have observed the pro-apoptotic potential of activated AMPK [30–33]. In this report, we found a gradual increase in the levels of AMPK phosphorylation in *Mapo1*-proficient cells after MNU treatment, implying a possible involvement of the activation of AMPK in the MNU-induced apoptosis pathway. In *Mapo1*-deficient cells, AMPK activation in this manner was hardly detectable, even after the treatment with MNU. Furthermore, the treatment of cells with AICAR, a specific activator of AMPK, resulted in AMPKα phosphorylation and mitochondrial membrane depolarization in a *Mapo1*-dependent manner. These findings extended onto the case of *Flcn*-knockdown cells. Taken together, it is likely that MAPO1 and FLCN positively regulate the activation of AMPK through their mutual interaction in the apoptotic signaling pathway, triggered by an alkylating agent. MAPO1 and FLCN proteins have been reported to undergo some modifications in cells [17,24]. The treatment with an alkylating agent might affect the modified states of these proteins, and might cause the activation of the protein complex, thus leading to AMPK activation. Another folliculin-interacting protein, FNIP1, which is homologous to MAPO1, is also capable of binding to AMPK [17]. The activation of AMPK might therefore be regulated in more complex ways under the balance of MAPO1 and FNIP1 activities.

Another important problem which remains to be solved is how the AMPK–MAPO1–FLCN complex is activated by the signal delivered from the mismatch repair protein complex, which itself is activated through the interaction with DNA carrying base mismatches. The signal may be delivered by direct physical contact between the two complexes or through the involvement of other protein factors. The protein linking analyses, aided by mass spectrometry, have been performed, but no evidence to show the physical association of the two complexes was obtained (unpublished results). It seems likely, therefore, that some other protein factor(s) might be involved in the signal transduction process. To identify such factors, it would be relevant to extend this approach using retrovirus-mediated gene-trap mutagenesis studies.

Germline mutations in the *FLCN* gene have been identified in patients with Birt-Hogg-Dubé (BHD) syndrome, which is an autosomal dominant disorder characterized by hamartomas of skin follicles, spontaneous pneumothorax, and renal tumors [20–22]. Furthermore, *BHD* heterozygous knockout mice were revealed to develop kidney cysts and tumors as they aged, while *BHD* homozygous null mice displayed early embryonic lethality [34,35]. The recent findings, including this report, strongly suggest that folliculin has physical and/or functional interactions with the AMPK-mTOR signaling pathway [17,34,36]. Mutations in several other tumor suppressor genes, such as *LKB1*, *TSC1* and *TSC2* [29,37], have also been shown to lead to dysregulation of AMPK-mTOR signaling and to the development of other hamartomatous syndromes. Our present findings that folliculin is involved in the induction of apoptosis might shed some light on the physiological roles of *BHD/FLCN* and other related tumor suppressor genes. We are currently establishing *Mapo1* knockout mice to analyze the possible roles of the gene in the suppression of tumor predisposition resulting from environmental stresses.

Conflict of interest statement

The authors declare that there are no conflicts of interests.

Acknowledgments

We thank Drs. H. Hayakawa and Y. Takagi (Fukuoka Dental College, Japan) for helpful discussion. This work was supported by grants (including a Frontier Research Grant) from the Ministry of Education, Culture, Sports, Science and Technology of Japan, and from the Ministry of Health, Labor and Welfare of Japan.

References

[1] D.T. Beranek, Distribution of methyl and ethyl adducts following alkylation with monofunctional alkylating agents, Mutat. Res. 231 (1990) 11–30.
[2] C. Coulondre, J.H. Miller, Genetic studies of the lac repressor. IV. Mutagenic specificity in the lacI gene of *Escherichia coli*, J. Mol. Biol. 117 (1977) 577–606.
[3] T. Ito, T. Nakamura, H. Maki, M. Sekiguchi, Roles of transcription and repair in alkylation mutagenesis, Mutat. Res. 314 (1994) 273–285.
[4] B. Demple, A. Jacobsson, M. Olsson, P. Robins, T. Lindahl, Repair of alkylated DNA in *Escherichia coli*. Physical properties of O6-methylguanine–DNA methyltransferase, J. Biol. Chem. 257 (1982) 13776–13780.
[5] H. Kawate, K. Ihara, K. Kohda, K. Sakumi, M. Sekiguchi, Mouse methyltransferase for repair of O6-methylguanine and O4-methylthymine in DNA, Carcinogenesis 16 (1995) 1595–1602.
[6] P. Branch, G. Aquilina, M. Bignami, P. Karran, Defective mismatch binding and a mutator phenotype in cells tolerant to DNA damage, Nature 362 (1993) 652–654.
[7] M. Hidaka, Y. Takagi, T.Y. Takano, M. Sekiguchi, PCNA-MutSalpha-mediated binding of MutLalpha to replicative DNA with mismatched bases to induce apoptosis in human cells, Nucleic Acids Res. 33 (2005) 5703–5712.
[8] A. Kat, W.G. Thilly, W.H. Fang, M.J. Longley, G.M. Li, P. Modrich, An alkylation-tolerant, mutator human cell line is deficient in strand-specific mismatch repair, Proc. Natl. Acad. Sci. U.S.A. 90 (1993) 6424–6428.
[9] B.J. Glassner, G. Weeda, J.M. Allan, J.L. Broekhof, N.H. Carls, I. Donker, B.P. Engelward, R.J. Hampson, R. Hersmus, M.J. Hickman, R.B. Roth, H.B. Warren, M.M. Wu, J.H. Hoeijmakers, L.D. Samson, DNA repair methyltransferase (Mgmt) knockout mice are sensitive to the lethal effects of chemotherapeutic alkylating agents, Mutagenesis 14 (1999) 339–347.
[10] K. Sakumi, A. Shiraishi, S. Shimizu, T. Tsuzuki, T. Ishikawa, M. Sekiguchi, Methylnitrosourea-induced tumorigenesis in MGMT gene knockout mice, Cancer Res. 57 (1997) 2415–2418.
[11] A. Shiraishi, K. Sakumi, M. Sekiguchi, Increased susceptibility to chemotherapeutic alkylating agents of mice deficient in DNA repair methyltransferase, Carcinogenesis 21 (2000) 1879–1883.
[12] T. Tsuzuki, K. Sakumi, A. Shiraishi, H. Kawate, H. Igarashi, T. Iwakuma, Y. Tominaga, S. Zhang, S. Shimizu, T. Ishikawa, et al., Targeted disruption of the DNA repair methyltransferase gene renders mice hypersensitive to alkylating agent, Carcinogenesis 17 (1996) 1215–1220.
[13] H. Kawate, K. Sakumi, T. Tsuzuki, Y. Nakatsuru, T. Ishikawa, S. Takahashi, H. Takano, T. Noda, M. Sekiguchi, Separation of killing and tumorigenic effects of an alkylating agent in mice defective in two of the DNA repair genes, Proc. Natl. Acad. Sci. U.S.A. 95 (1998) 5116–5120.
[14] Y. Takagi, M. Takahashi, M. Sanada, R. Ito, M. Yamaizumi, M. Sekiguchi, Roles of MGMT and MLH1 proteins in alkylation-induced apoptosis and mutagenesis, DNA Repair (Amst.) 2 (2003) 1135–1146.
[15] K. Ochs, B. Kaina, Apoptosis induced by DNA damage O6-methylguanine is Bcl-2 and caspase-9/3 regulated and Fas/Caspase-8 independent, Cancer Res. 60 (2000) 5815–5824.
[16] K. Komori, Y. Takagi, M. Sanada, T.H. Lim, Y. Nakatsu, T. Tsuzuki, M. Sekiguchi, M. Hidaka, A novel protein, MAPO1, that functions in apoptosis triggered by O6-methylguanine mispair in DNA, Oncogene 28 (2009) 1142–1150.
[17] M. Baba, S.B. Hong, N. Sharma, M.B. Warren, M.L. Nickerson, A. Iwamatsu, D. Esposito, W.K. Gillette, R.F. Hopkins 3rd, J.L. Hartley, M. Furihata, S. Oishi, W. Zhen, T.R. Burke, W.M. Linehan Jr., L.S. Schmidt, B. Zbar, Folliculin encoded

by the BHD gene interacts with a binding protein, FNIP1, and AMPK and is involved in AMPK and mTOR signaling, Proc. Natl. Acad. Sci. U.S.A. 103 (2006) 15552–15557.
[18] M.L. Nickerson, M.B. Warren, J.R. Toro, V. Matrosova, G. Glenn, M.L. Turner, P. Duray, M. Merino, P. Choyke, C.P. Pavlovich, N. Sharma, M. Walther, D. Munroe, R. Hill, E. Maher, C. Greenberg, M.I. Lerman, W.M. Linehan, B. Zbar, L.S. Schmidt, Mutations in a novel gene lead to kidney tumors, lung wall defects, and benign tumors of the hair follicle in patients with the Birt-Hogg-Dube syndrome, Cancer Cell 2 (2002) 157–164.
[19] C.D. Vocke, Y. Yang, C.P. Pavlovich, L.S. Schmidt, M.L. Nickerson, C.A. Torres-Cabala, M.J. Merino, M.M. Walther, B. Zbar, W.M. Linehan, High frequency of somatic frameshift BHD gene mutations in Birt-Hogg-Dube-associated renal tumors, J. Natl. Cancer Inst. 97 (2005) 931–935.
[20] A.R. Birt, G.R. Hogg, W.J. Dube, Hereditary multiple fibrofolliculomas with trichodiscomas and acrochordons, Arch. Dermatol. 113 (1977) 1674–1677.
[21] J.R. Toro, G. Glenn, P. Duray, T. Darling, G. Weirich, B. Zbar, M. Linehan, M.L. Turner, Birt-Hogg-Dube syndrome: a novel marker of kidney neoplasia, Arch. Dermatol. 135 (1999) 1195–1202.
[22] B. Zbar, W.G. Alvord, G. Glenn, M. Turner, C.P. Pavlovich, L. Schmidt, M. Walther, P. Choyke, G. Weirich, S.M. Hewitt, P. Duray, F. Gabril, C. Greenberg, M.J. Merino, J. Toro, W.M. Linehan, Risk of renal and colonic neoplasms and spontaneous pneumothorax in the Birt-Hogg-Dube syndrome, Cancer Epidemiol. Biomarkers Prev. 11 (2002) 393–400.
[23] H. Hasumi, M. Baba, S.B. Hong, Y. Hasumi, Y. Huang, M. Yao, V.A. Valera, W.M. Linehan, L.S. Schmidt, Identification and characterization of a novel folliculin-interacting protein FNIP2, Gene 415 (2008) 60–67.
[24] Y. Takagi, T. Kobayashi, M. Shiono, L. Wang, X. Piao, G. Sun, D. Zhang, M. Abe, Y. Hagiwara, K. Takahashi, O. Hino, Interaction of folliculin (Birt-Hogg-Dube gene product) with a novel Fnip1-like (FnipL/Fnip2) protein, Oncogene 27 (2008) 5339–5347.
[25] D. Carling, The AMP-activated protein kinase cascade – a unifying system for energy control, Trends Biochem. Sci. 29 (2004) 18–24.
[26] D.G. Hardie, The AMP-activated protein kinase pathway – new players upstream and downstream, J. Cell Sci. 117 (2004) 5479–5487.
[27] S.A. Hawley, M. Davison, A. Woods, S.P. Davies, R.K. Beri, D. Carling, D.G. Hardie, Characterization of the AMP-activated protein kinase from rat liver and identification of threonine 172 as the major site at which it phosphorylates AMP-activated protein kinase, J. Biol. Chem. 271 (1996) 27879–27887.
[28] J.M. Lizcano, O. Goransson, R. Toth, M. Deak, N.A. Morrice, J. Boudeau, S.A. Hawley, L. Udd, T.P. Makela, D.G. Hardie, D.R. Alessi, LKB1 is a master kinase that activates 13 kinases of the AMPK subfamily, including MARK/PAR-1, EMBO J. 23 (2004) 833–843.
[29] R.J. Shaw, M. Kosmatka, N. Bardeesy, R.L. Hurley, L.A. Witters, R.A. DePinho, L.C. Cantley, The tumor suppressor LKB1 kinase directly activates AMP-activated kinase and regulates apoptosis in response to energy stress, Proc. Natl. Acad. Sci. U.S.A. 101 (2004) 3329–3335.
[30] C. Cao, S. Lu, R. Kivlin, B. Wallin, E. Card, A. Bagdasarian, T. Tamakloe, W.M. Chu, K.L. Guan, Y. Wan, AMP-activated protein kinase contributes to UV- and H2O2-induced apoptosis in human skin keratinocytes, J. Biol. Chem. 283 (2008) 28897–28908.
[31] R.G. Jones, D.R. Plas, S. Kubek, M. Buzzai, J. Mu, Y. Xu, M.J. Birnbaum, C.B. Thompson, AMP-activated protein kinase induces a p53-dependent metabolic checkpoint, Mol. Cell 18 (2005) 283–293.
[32] R. Okoshi, T. Ozaki, H. Yamamoto, K. Ando, N. Koida, S. Ono, T. Koda, T. Kamijo, A. Nakagawara, H. Kizaki, Activation of AMP-activated protein kinase induces p53-dependent apoptotic cell death in response to energetic stress, J. Biol. Chem. 283 (2008) 3979–3987.
[33] W.B. Zhang, Z. Wang, F. Shu, Y.H. Jin, H.Y. Liu, Q.J. Wang, Y. Yang, Activation of AMP-activated protein kinase by temozolomide contributes to apoptosis in glioblastoma cells via p53 activation and mTORC1 inhibition, J. Biol. Chem. 285 (2010) 40461–40471.
[34] T.R. Hartman, E. Nicolas, A. Klein-Szanto, T. Al-Saleem, T.P. Cash, M.C. Simon, E.P. Henske, The role of the Birt-Hogg-Dube protein in mTOR activation and renal tumorigenesis, Oncogene 28 (2009) 1594–1604.
[35] Y. Hasumi, M. Baba, R. Ajima, H. Hasumi, V.A. Valera, M.E. Klein, D.C. Haines, M.J. Merino, S.B. Hong, T.P. Yamaguchi, L.S. Schmidt, W.M. Linehan, Homozygous loss of BHD causes early embryonic lethality and kidney tumor development with activation of mTORC1 and mTORC2, Proc. Natl. Acad. Sci. U.S.A. 106 (2009) 18722–18727.
[36] X. Piao, T. Kobayashi, L. Wang, M. Shiono, Y. Takagi, G. Sun, M. Abe, Y. Hagiwara, D. Zhang, K. Okimoto, M. Kouchi, I. Matsumoto, O. Hino, Regulation of folliculin (the BHD gene product) phosphorylation by Tsc2-mTOR pathway, Biochem. Biophys. Res. Commun. 389 (2009) 16–21.
[37] K. Inoki, M.N. Corradetti, K.L. Guan, Dysregulation of the TSC-mTOR pathway in human disease, Nat. Genet. 37 (2005) 19–24.

$SCF^{\beta TrCP}$ mediates stress-activated MAPK-induced Cdc25B degradation

Sanae Uchida[1], Nobumoto Watanabe[2], Yasusei Kudo[3], Katsuji Yoshioka[4], Tsukasa Matsunaga[5], Yukihito Ishizaka[6], Hitoshi Nakagama[7], Randy Y. C. Poon[8] and Katsumi Yamashita[5,*]

[1]Venture Business Laboratory, Center for Innovation, Kanazawa University, Kakuma, Kanazawa 920-1192, Ishikawa, Japan
[2]Chemical Library Validation Team, Chemical Biology Core Facility, Chemical Biology Department, RIKEN ASI, Wako 351-0198, Saitama, Japan
[3]Department of Oral Maxillofacial Pathobiology, Division of Frontier Medical Science, Graduate School of Medical Sciences, Hiroshima University, Hiroshima 734-8553, Japan
[4]Division of Molecular Cell Signaling, Cancer Research Institute, Kanazawa University, Kakuma, Kanazawa 920-1192, Ishikawa, Japan
[5]Division of Pharmaceutical Sciences, Institute of Medical, Pharmaceutical and Health Sciences, Kanazawa University, Kakuma, Kanazawa 920-1192, Ishikawa, Japan
[6]Division of Intractable Diseases, Research Institute, National Center for Global Health and Medicine, Tokyo 162-8655, Japan
[7]Early Oncogenesis Research Project, National Cancer Center Research Institute, Tokyo 104-0045, Japan
[8]Division of Life Science, The Hong Kong University of Science and Technology, Clear Water Bay, Hong Kong
*Author for correspondence (katsumi@kenroku.kanazawa-u.ac.jp)

Accepted 26 April 2011
Journal of Cell Science 124, 2816-2825

doi:10.1242/jcs.083931

Summary

Cdc25A, which is one of the three mammalian CDK-activating Cdc25 protein phosphatases (Cdc25A, B and C), is degraded through $SCF^{\beta TrCP}$-mediated ubiquitylation following genomic insult; however, the regulation of the stability of the other two Cdc25 proteins is not well understood. Previously, we showed that Cdc25B is primarily degraded by cellular stresses that activate stress-activated MAPKs, such as Jun NH_2-terminal kinase (JNK) and p38. Here, we report that Cdc25B was ubiquitylated by $SCF^{\beta TrCP}$ E3 ligase upon phosphorylation at two Ser residues in the βTrCP-binding-motif-like sequence $D^{94}AGLCMDSPSP^{104}$. Point mutation of these Ser residues to alanine (Ala) abolished the JNK-induced ubiquitylation by $SCF^{\beta TrCP}$, and point mutation of DAG to AAG or DAA eradicated both βTrCP binding and ubiquitylation. Further analysis of the mode of βTrCP binding to this region revealed that the PEST-like sequence from $E^{82}SS$ to $D^{94}AG$ is crucially involved in both the βTrCP binding and ubiquitylation of Cdc25B. Furthermore, the phospho-mimetic replacement of all 10 Ser residues in the $E^{82}SS$ to $SPSP^{104}$ region with Asp resulted in βTrCP binding. Collectively, these results indicate that stress-induced Cdc25B ubiquitylation by $SCF^{\beta TrCP}$ requires the phosphorylation of $S^{101}PS^{103}P$ in the βTrCP-binding-motif-like and adjacent PEST-like sequences.

Key words: Cdc25B, $SCF^{\beta TrCP}$, Phosphorylation, PEST-like

Introduction

Cdc25 dual-specificity phosphatases promote cell cycle progression via the activation of cyclin-dependent kinase (CDK)–cyclin by removing inhibitory phosphate groups on CDK (Morgan, 1995; Boutros et al., 2006). Higher Metazoa possess three isoforms of Cdc25: Cdc25A, B and C. These are largely considered to serve roles in different phases of the cell cycle: Cdc25A in the G1 to S phase, and Cdc25B and C in the G2 to M phase (Boutros et al., 2006). However, this is not strictly correct because the depletion of either one or two *Cdc25* genes does not produce a defective phenotype in the normal cell cycle, indicating that their roles overlap in somatic cell-cycle control (Chen et al., 2001; Lincoln et al., 2002; Ferguson et al., 2005; Ray et al., 2007; Lee et al., 2009).

Of the three mammalian Cdc25 isoforms, Cdc25A has received special attention because it is a target of the DNA replication or damage checkpoint (Donzelli and Draetta, 2003; Bartek et al., 2004) and is the only Cdc25 that is essential to mouse embryogenesis (Ray et al., 2007; Lee et al., 2009). Cdc25A is phosphorylated rapidly by CHK1 upon genomic damage or replication arrest, and this is followed by the phosphorylation of crucial Ser residues in the βTrCP-binding DSG (Asp-Ser-Gly) motif by NEK11 (Busino et al., 2003; Jin et al., 2003; Melixetian et al., 2009), which initiates $SCF^{\beta TrCP}$-mediated ubiquitylation and degradation (Busino et al., 2004). Moreover, Cdc25A is directly linked to tumorigenesis, and the frequent overexpression of Cdc25A in human cancers is well documented (Kristjansdottir and Rudolph, 2004; Boutros et al., 2007).

The WD repeat-containing F-box protein βTrCP is a substrate-binding component of SCF (Skp1–cullin-1–F-box protein) E3 ubiquitin ligase that recognises the doubly phosphorylated conserved motif DSGxxS (S can be replaced by T, and x represents any amino acid) (Winston et al., 1999; Latres et al., 1999). $SCF^{\beta TrCP}$ targets a number of proteins that regulate the cell cycle and apoptosis (Frescas and Pagano, 2008). In particular, some proteins that control the G2–M transition, such as Cdc25A, Emi1, Wee1A and Bora, are $SCF^{\beta TrCP}$ substrates, and most of them contain the above-mentioned βTrCP-binding sequence (Busino et al., 2003; Jin et al., 2003; Margottin-Goguet et al., 2003; Guardavaccaro et al., 2003; Watanabe et al., 2004; Seki et al., 2008). Wee1 kinase is also a substrate of $SCF^{\beta TrCP}$, but its proposed βTrCP-binding sequence deviates from the consensus sequence (Watanabe et al., 2004). The consensus sequence and its deviated phosphopeptides bind βTrCP by forming hydrogen bonds and electrostatic interactions (Wu et al., 2003). In addition to such phosphopeptides, Cdc25A and Cdc25B possess the non-phosphorylated βTrCP-binding sequence DDGxxD (Kanemori et al., 2005).

Similar to Cdc25A, Cdc25B can transform retinoblastoma-protein-negative cells or normal cells when coexpressed with the oncogenic Ras (Galaktionov et al., 1995). Cdc25B overexpression is also found in human cancers and is correlated with a poor prognosis, as in the case of Cdc25A (Kristjansdottir and Rudolph, 2004; Boutros et al., 2007). The tumorigenic activity of Cdc25B is partly explained by an increase in hyperplasia or susceptibility to carcinogens in Cdc25B transgenic mice (Ma et al., 1999; Yao et al., 1999). Moreover, Cdc25B overexpression accelerates mitotic entry (Karlsson et al., 1999) and overrides the radiation-induced G2 checkpoint in vitro (Miyata et al., 2001).

Recently, we showed that Cdc25B is degraded rapidly by non-genotoxic stimuli that activate stress-responsive MAPKs, such as Jun N-terminal kinase (JNK) and p38 (Uchida et al., 2009). Our results suggested that these kinases phosphorylate specific Ser residues in the N-terminal region (S101 and S103) to induce Cdc25B degradation. We also found that HeLa cells expressing the non-phosphorylatable S101A mutant Cdc25B were more refractory to anisomycin-induced G2 arrest than wild-type HeLa cells.

Here, we report that JNK-induced Cdc25B ubiquitylation is mediated by the F-box protein βTrCP-containing SCF ubiquitin ligase. We show that S101 and S103 are phosphorylated upon non-genotoxic stress and that βTrCP binds the sequence around S101 and S103 of Cdc25B in a phosphorylation-dependent manner, even when the DSG consensus βTrCP-binding sequence is replaced with DAG. Our data also indicate that full binding and ubiquitylation of Cdc25B by SCF$^{\beta TrCP}$ requires an upstream ESS (Glu-Ser-Ser)-rich PEST-like sequence, as well as DAG and S101 and S103 phosphorylation.

Results

Ubiquitylation of Cdc25B is carried out by SCF$^{\beta TrCP}$ and is controlled by JNK

Our previous report suggested that non-genotoxic stress-induced Cdc25B degradation was mediated by the ubiquitin–proteasome pathway via S101 and S103 phosphorylation by JNK or p38 (Uchida et al., 2009). Fig. 1A shows that the amino acid sequence surrounding S101 and S103 of Cdc25B is similar to that in Cdc25A, which is a substrate of SCF$^{\beta TrCP}$ E3 ubiquitin ligase (Busino et al., 2003; Jin et al., 2003). Despite the overall similarity, the crucial βTrCP-binding motif of Cdc25A (DSG) is replaced with DAG in Cdc25B, and DAG is reported to be inactive for βTrCP binding in humans and *Xenopus* Cdc25A (Busino et al., 2003; Jin et al., 2003; Kanemori et al., 2005).

The corresponding region of Cdc25B, including the human splice variants Cdc25B2 and Cdc25B3 and mouse Cdc25B1, has a similar amino acid sequence (Fig. 1A) (Baldin et al., 1997; Kakizuka et al., 1992). As indicated in Fig. 1B, human Cdc25B3,

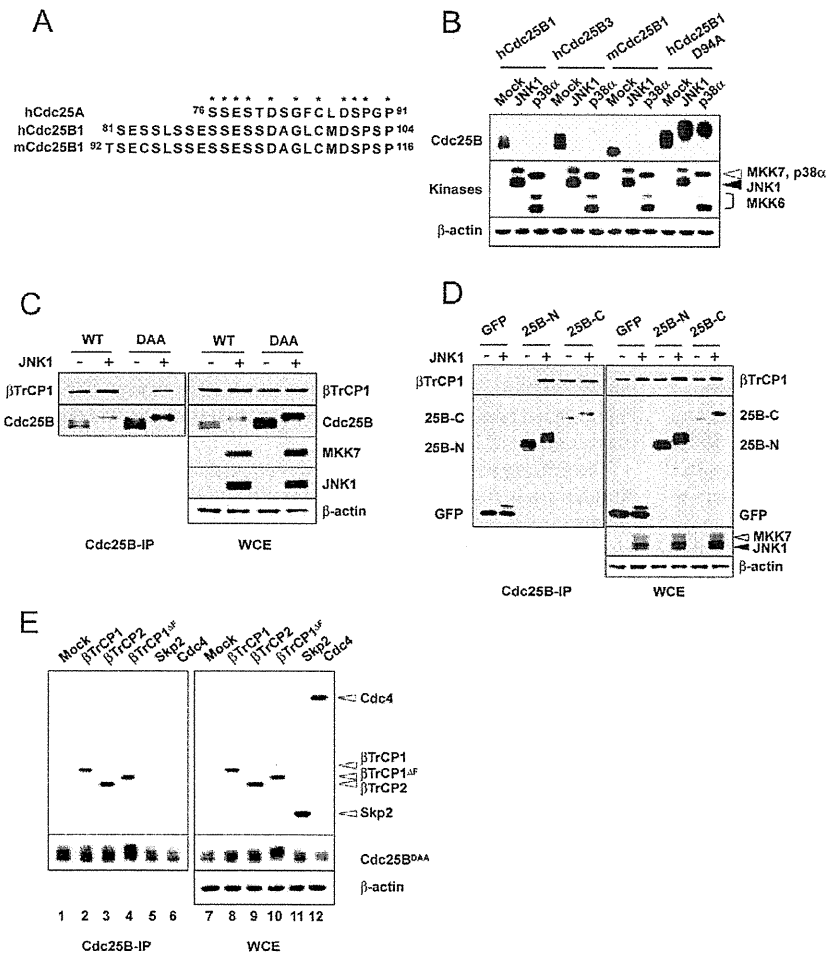

Fig. 1. βTrCP binds Cdc25B. (**A**) The aligned amino acid sequences of human (h) and mouse (m) Cdc25B and human Cdc25A, required for βTrCP binding. Asterisks indicate amino acids common to all three peptides. (**B**) Each FLAG-tagged cDNA of human Cdc25B1 and B3 and mouse Cdc25B1 was co-transfected with either JNK1 and its activator MKK7 or p38α and its activator MKK6, followed by immunoblotting to detect the expression of the indicated proteins (JNK1 or p38α was co-transfected with its respective activator, MKK7 or MKK6, unless stated otherwise and the coexpression of JNK1 and MKK7 or p38α with MKK6 is shown as JNK1 or p38, respectively, thereafter). The expression of human Cdc25B1 with a mutation at D94 to A of DAG (D94A) was also determined. (**C**) Either a FLAG–Cdc25B^{WT} or FLAG–Cdc25B^{DAA} with mutations in the constitutive βTrCP-binding sequence DDG was co-transfected with Myc-βTrCP1 in the presence or absence of JNK1. Then, 24 hours later, either Cdc25B binding to βTrCP1 or recovered Cdc25B was determined by immunoprecipitation with anti-FLAG beads, followed by immunoblotting with anti-Myc or anti-FLAG antibodies (Cdc25B-IP lanes). The expression of the indicated proteins is also shown (WCE lanes). (**D**) The βTrCP1 binding to Cdc25B fragments of the N-terminal 175 amino acids (1–175; 25B–N) or C-terminal fragment (180–580; 25B–C), both of which contain an N-terminal FLAG tag and C-terminal GFP tag, was examined as described in C. FLAG–GFP was used as a control (Cdc25B-IP lanes). The expression of the indicated proteins is shown (WCE lanes). (**E**) FLAG–Cdc25B^{DAA} and Myc-tagged F-box proteins were co-transfected and their interaction was determined by immunoprecipitation and immunoblotting. The interaction between Cdc25B^{DDA} and βTrCP1$^{\Delta F}$ lacking an F-box sequence was also determined (Cdc25B-IP lanes). The expression of the indicated proteins is also shown (WCE lanes).

mouse Cdc25B1 and human Cdc25B1 were also degraded on coexpression with JNK or p38 (hereafter, we refer to human Cdc25B1 as Cdc25B). Interestingly, the Cdc25B D94A mutant was refractory to JNK- or p38-induced degradation, suggesting the involvement of βTrCP binding (Fig. 1B).

Next, we investigated the JNK-dependent interaction between βTrCP1 and Cdc25B. We compared βTrCP binding to the Cdc25B of the wild type and a mutant that lacked the constitutive βTrCP-binding motif by mutating $D^{254}DG$ to DAA, which hereafter is referred to as $Cdc25B^{DAA}$. Although wild-type Cdc25B bound βTrCP1 irrespective of the JNK activity, $Cdc25B^{DAA}$ interacted with βTrCP1 in a JNK-dependent manner (Fig. 1C). JNK induced wild-type Cdc25B degradation and apparent Cdc25B binding was not enhanced. Given the JNK-induced wild-type Cdc25B degradation that occurred, several times more βTrCP was estimated to bind Cdc25B on coexpression with JNK. Likewise, the Cdc25B N-terminal fragment displayed JNK-dependent βTrCP1 binding, whereas the C-terminal fragment with the DDG site showed that βTrCP bound in a JNK-independent manner (Fig. 1D). Furthermore, $Cdc25B^{DAA}$ interacted with βTrCP1 and βTrCP2, but not with other F-box proteins such as Skp2 and Cdc4 (Fig. 1E). $Cdc25B^{DAA}$ was stabilised when co-transfected with the F-box deletion mutant $βTrCP1^{ΔF}$, which lacks ubiquitylation activity because of its inability to bind to the core SCF complex, but retains substrate-binding ability via an intact WD domain (Fig. 1E).

Next, we investigated the ubiquitylation of Cdc25B by $SCF^{βTrCP}$ in vitro. ^{35}S-labelled $Cdc25B^{DAA}$ was efficiently ubiquitylated by SCF containing βTrCP1 or βTrCP2, in a JNK-dependent manner. By contrast, no ubiquitylated signal was detected when Skp2 or Cdc4 was used as the F-box protein (Fig. 2A). Furthermore, $βTrCP1^{ΔF}$ did not ubiquitylate Cdc25B (Fig. 2B). Note that $SCF^{βTrCP1}$ and $SCF^{βTrCP2}$ could ubiquitylate $Cdc25B^{DAA}$ without JNK, but JNK clearly enhanced the ubiquitylation (Fig. 2A,B). A high level of ubiquitylation was observed in the absence of JNK when wild-type Cdc25B was used for the in vitro ubiquitylation assay (Fig. 2C). Nevertheless, slight enhancement of Cdc25B ubiquitylation by $SCF^{βTrCP1}$ was observed in the presence of JNK activity (Fig. 2C). These results indicate that $SCF^{βTrCP}$ binds and ubiquitylates Cdc25B in a JNK-dependent manner, which is independent of the DDG constitutive binding site, and that a new JNK-regulated βTrCP-binding site is located in the N-terminal 175 amino acids of Cdc25B.

Our previous investigation suggested that S101 and S103 were possible target sites of JNK or p38 (Uchida et al., 2009). Therefore, we assessed the contributions of S101 and S103 to $SCF^{βTrCP}$-mediated $Cdc25B^{DAA}$ ubiquitylation. As indicated in Fig. 2D, whereas the ubiquitylation of Cdc25B was greatly compromised by S101A or S103A mutations, it was almost completely abolished with a S101A, S103A double mutant. These results indicate that the effects of S101 and S103 on Cdc25B ubiquitylation were collaborative. Other Cdc25B proteins, such as human Cdc25B3 and mouse Cdc25B1, were also ubiquitylated by $SCF^{βTrCP1}$ in the presence of JNK1 (supplementary material Fig. S1A). Intriguingly, $Cdc25B^{D94A}$ was hardly ubiquitylated (supplementary material Fig. S1A), suggesting that D94 in DAG is involved in JNK-induced Cdc25B ubiquitylation. Moreover, in such wild-type or mutant Cdc25B, βTrCP1 binding to Cdc25B proteins were roughly proportional to their ubiquitylation level (supplementary material Fig. S1B). Collectively, these results clearly indicate that JNK-induced Cdc25B degradation is mediated by $SCF^{βTrCP1}$, and that the phosphorylation of Cdc25B S101 and S103 plays an important role in this process.

JNK-induced Cdc25B degradation is aborted by βTrCP depletion

Next, we assessed the effects of βTrCP depletion on JNK-induced Cdc25B degradation using siRNA that targets both βTrCP1 and βTrCP2. We used either one siRNA, used in previous investigations

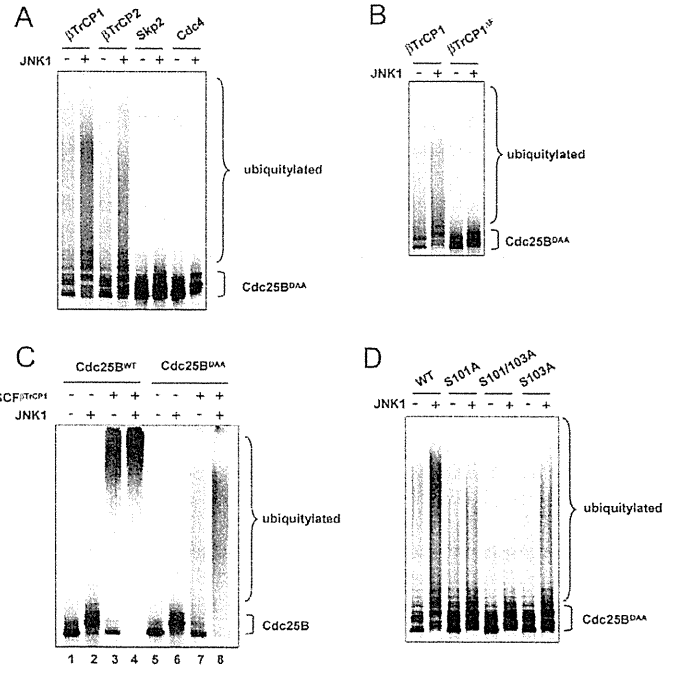

Fig. 2. Cdc25B is ubiquitylated by $SCF^{βTrCP}$ in vitro.
(**A**) [^{35}S]methionine-labelled $Cdc25B^{DAA}$ was incubated with each SCF complex in the presence or absence of JNK1, and ubiquitylation was determined as described in the Materials and Methods.
(**B**) [^{35}S]methionine-labelled $Cdc25B^{DAA}$ was incubated with each $SCF^{βTrCP1}$ or $SCF^{ΔβTrCP1}$ complex in the presence or absence of JNK1, and ubiquitylation was determined as described in A. (**C**) $SCF^{βTrCP1}$-mediated ubiquitylation of [^{35}S]methionine-labelled $Cdc25B^{WT}$ (wild type) or $Cdc25B^{DAA}$ was determined as described in A.
(**D**) [^{35}S]methionine-labelled $Cdc25B^{DAA}$ S101 and S103 (wild type), or with a mutation of S101A, S103A, or S101A and S103A (S101/103A), was incubated with $SCF^{βTrCP1}$ to determine ubiquitylation as described in A.

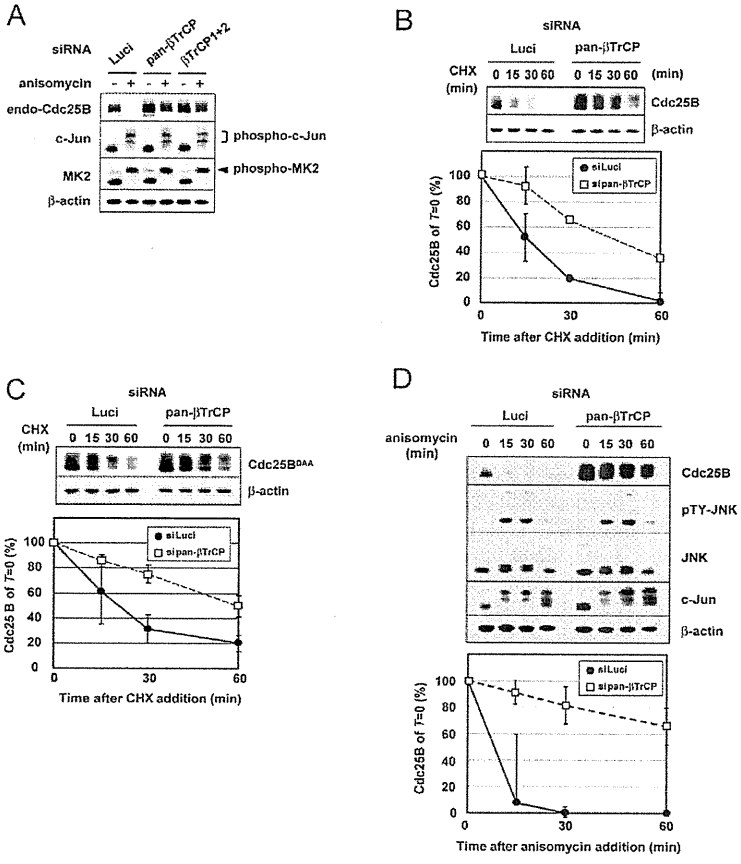

Fig. 3. βTrCP1 and 2 depletion stabilises Cdc25B. (**A**) HeLa cells were depleted of both βTrCP1 and 2 with siRNA (either pan-βTrCP or combined siRNA for βTrCP1 and 2). Luci indicates siRNA against luciferase, used as a control. After 24 hours, HeLa cells were treated with 50 ng/ml anisomycin for 30 minutes. The expression of endogenous Cdc25B was also determined by immunoprecipitation followed by immunoblotting. The expression of the other indicated proteins (Jun, MK2 and β-actin) was also determined by immunoblotting. (**B**) HeLa-W40 cells transfected with siRNA for either Luci or pan-βTrCP were treated with cycloheximide (CHX; 50 μg/ml), and expression of the indicated proteins was determined by immunoblotting at the indicated times. The relative Cdc25B expression is shown in the lower panel with the value at time 0 set at 100. The bars indicate the standard deviation (s.d.) of three independent experiments. (**C**) The expression of Cdc25B^{DAA} in HeLa-DAA34 cells in the presence of CHX was determined as described in B. (**D**) HeLa-W40 cells transfected with siRNA for either for Luci or pan-βTrCP were treated with 50 ng/ml anisomycin, and the expression of the indicated proteins was determined as described in B.

(Margottin-Goguet et al., 2003; Guardavaccaro et al., 2003) (denoted here as pan-βTrCP) or two in combination, which enabled us to knockdown either βTrCP1 or βTrCP2 specifically (denoted as βTrCP1 and 2). The effect on βTrCP depletion on introducing these siRNAs to HeLa-W40 cells that stably express FLAG–Cdc25B (Uchida et al., 2009) is shown in supplementary material Fig. S2A (we show only the expression of βTrCP1 because we had no specific antibody to βTrCP2). The results also indicated that the application of such siRNA to HeLa-W40 cells enhanced the expression of FLAG–Cdc25B and endogenous Cdc25A, suggesting that both Cdc25A and Cdc25B are destroyed via a βTrCP-mediated pathway, even in the absence of cellular stress (supplementary material Fig. S2A).

First, we examined the stability of endogenous Cdc25B after siRNA depletion of βTrCP1 and 2 with either siRNA for pan-βTrCP or combined siRNA for βTrCP1 and 2. As shown in Fig. 3A, βTrCP depletion substantially increased the resistance of endogenous Cdc25B under anisomycin stress. Moreover, transiently expressed Cdc25B^{DAA} also became refractory to the JNK-induced degradation on βTrCP1 and 2 depletion (supplementary material Fig. S2B). Because the depletion of βTrCP1 and 2 with the two siRNA treatments gave similar results (Fig. 3A and supplementary material Fig. S2A), we mainly used pan-βTrCP siRNA in the subsequent experiments.

Next, we asked whether the half-life of Cdc25B was affected by βTrCP depletion. HeLa-W40 cells stably expressing FLAG–Cdc25B were depleted of βTrCP1 and 2 with pan-βTrCP siRNA and the expression of Cdc25B protein was determined in the presence of cycloheximide. As indicated in Fig. 3B, wild-type Cdc25B appeared to be stabilised in βTrCP-depleted cells. Interestingly, the steady-state expression of constitutively expressed Cdc25B^{DAA} in HeLa-DAA34 cells was also less affected in βTrCP-depleted cells (Fig. 3C), suggesting that the SCF$^{\beta TrCP}$-mediated ubiquitin–proteasome pathway controls Cdc25B stability in unstressed conditions, through a site other than the DDG βTrCP-binding site.

We further investigated the involvement of βTrCP in anisomycin-induced Cdc25B degradation. FLAG–Cdc25B^{WT}-expressing HeLa-W40 cells were transfected with either luciferase or pan-βTrCP siRNA, followed by a 50 ng/ml anisomycin challenge. βTrCP1 and 2 depletion strongly compromised anisomycin-induced Cdc25B degradation (Fig. 3D). βTrCP depletion of FLAG–Cdc25B^{DAA}-expressing HeLa-DAA34 cells had similar effects (supplementary material Fig. S2B). Collectively, these results unequivocally indicate that SCF$^{\beta TrCP}$ directly controls the non-genotoxic stress-induced instability of Cdc25B. Furthermore, these results also suggest that a site other than the constitutive binding site DDG controls the steady-state stability of Cdc25B.

JNK phosphorylates Cdc25B under stressful conditions

Next, we investigated whether JNK or p38 phosphorylated S101 and S103 by raising antibodies that recognised S101-, S103- or S101 and S103-phosphorylated Cdc25B; the antibody specificity is shown in supplementary material Fig. S3A. Using these

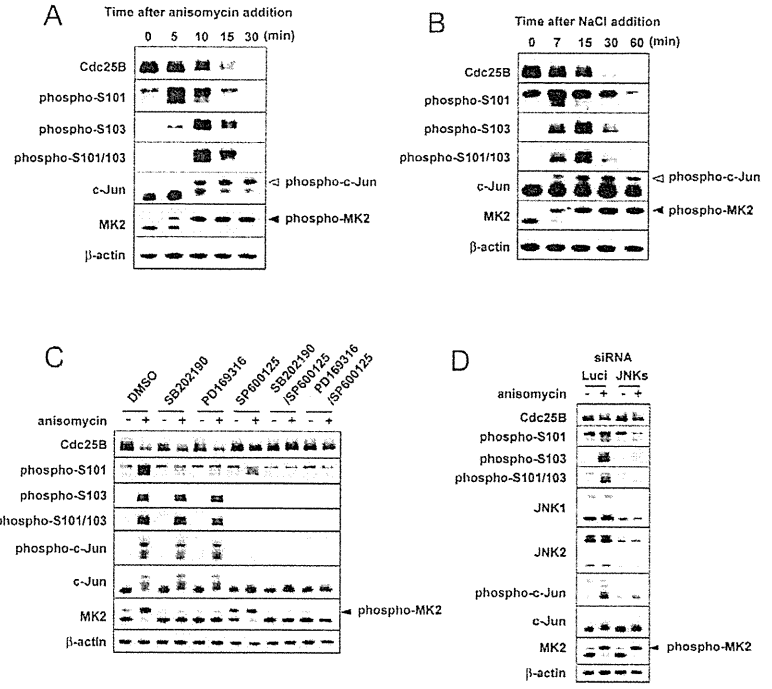

Fig. 4. Cdc25B S101 and S103 are phosphorylated by non-genotoxic insults. (**A**) HeLa-W40 cells that expressed FLAG–Cdc25B were treated with 50 ng/ml anisomycin. At the indicated times Cdc25B was immunoprecipitated, and phosphorylation was detected with antibodies. The expression of FLAG–Cdc25B, Jun, MK2 and β-actin are also shown. (**B**) HeLa-W40 cells were treated with 300 mM NaCl, and phosphorylation at S101 and S103 and the expression of the indicated proteins was detected, as described in A. (**C**) HeLa-W40 cells were treated with each inhibitor (5 μM each of SB202190 and PD169316 for p38 and 20 μM SP600125 for JNK, or a combination of SB and SP or PD and SP to inhibit p38 and JNK) 1 hour before the 50 ng/ml anisomycin challenge. Cell extracts were prepared after 10 minutes, and Cdc25B was immunoprecipitated. Phosphorylation at S101 and S103 and the expression of the indicated proteins were determined by immunoblotting. (**D**) HeLa-W40 cells were treated with siRNA for Luc or JNK (the siRNA for JNK was a mixture of one siJNK1 and two siJNK2). After 24 hours, the cells were treated with 50 ng/ml anisomycin for 10 minutes and cell extracts were prepared. The phosphorylation of Cdc25B at S101 and S103 and the expression of the indicated proteins were determined by immunoblotting.

antibodies, we investigated the phosphorylation status of S101 and S103 under either unstressed or stressed conditions. Conventional HeLa cells were not useful in these experiments because we could not recover enough Cdc25B by immunoprecipitation to detect its phosphorylation. We therefore used HeLa-W40 cells for phosphorylation analyses. Although a slight, but obvious, phosphorylated S101 (S101-*P*) signal was detected under unstressed conditions, S101 phosphorylation increased dramatically within 5 minutes of the 50 ng/ml anisomycin treatment, concomitant with p38 activation, as determined by the appearance of the phosphorylated form of MK2 (Fig. 4A). Unlike S101, the S103 phosphorylation signal was undetectable at time 0. A slight increase in phosphorylation was detected at 5 minutes and a much stronger signal was detected at 10 minutes, at which point JNK was fully activated, as determined by the Jun-*P* signal. The results for S103-*P* were similar to those for S101 and S103 double phosphorylation, for which the maximum level was detected at 10 minutes. Cdc25B phosphorylation decreased at 15 minutes and disappeared completely thereafter as a result of Cdc25B degradation. Similar results were obtained when stress was induced with 300 mM NaCl (Fig. 4B) or ultraviolet (UV) irradiation (supplementary material Fig. S3B). The steady-state phosphorylation of S101 and the similarity in the pattern between S103-*P* and the double S101-*P* and S103-*P* suggest that the phosphorylation of S103 occurs in S101-phosphorylated Cdc25B, because S101 is always phosphorylated in the absence of stress.

Next, we investigated the effects of the p38 inhibitors SB202190 and PD169316 (abbreviated to SB and PD, respectively) or the JNK inhibitors SP600125 (abbreviated to SP) on Cdc25B phosphorylation in HeLa-W40 cells. First, we determined suitable concentrations of these inhibitors for the specific inhibition of the respective kinases, because these kinases are often cross-inhibited by such inhibitors. As shown in supplementary material Fig. S4A, 20 μM SB inhibited both p38 and JNK activity, as determined by the disappearance of the phosphorylated MK2 and phosphorylated Jun signals, respectively, and it specifically inhibited p38 at a concentration as low as 5 μM without JNK inhibition. Supplementary material Fig. S4B,C also shows that 5 μM PD and 20 μM SP are suitable for the specific inhibition of p38 and JNK, respectively, without obvious cross-inhibition. As indicated in Fig. 4C, anisomycin-induced S101 phosphorylation was reduced by the p38 inhibitors SB and PD, but these inhibitors did not affect S103 phosphorylation. However, the JNK inhibitor SP completely inhibited S103, and modest inhibition of S101 phosphorylation was also observed. The role of JNK in S103 and S101 phosphorylation was also indicated by the siRNA depletion of JNK1 and JNK2 in anisomycin-treated HeLa-W40 cells, where the S101-*P* signal was reduced and the S101-*P*-103-*P* signal was almost completely abolished by the knockdown of both JNK1 and 2 (Fig. 4D). In a similar context, the clear reduction of the expression of endogenous Cdc25B by the transfection of wild-type, but not the kinase-dead mutant JNK1, also suggests that JNK functions in the degradation of endogenous Cdc25B (supplementary material Fig. S4D).

Collectively, these and our previous results indicate that the enhanced phosphorylation at S101 caused by p38 and JNK and de novo phosphorylation of S103 by JNK play crucial roles in stress-induced Cdc25B degradation. Furthermore, the S101-*P* signal detected under unstressed conditions did not disappear completely with the p38 inhibitors or JNK inhibitor, suggesting that an unidentified kinase(s) that phosphorylates S101 is involved in steady-state Cdc25B degradation.

The βTrCP-binding-motif-like DAG is essential for $SCF^{\beta TrCP}$-mediated Cdc25B ubiquitylation

The above results suggested that DAG, previously believed to be inactive, is functional in βTrCP-mediated Cdc25B ubiquitylation. To explore this possibility, we made a mutant Cdc25B in which

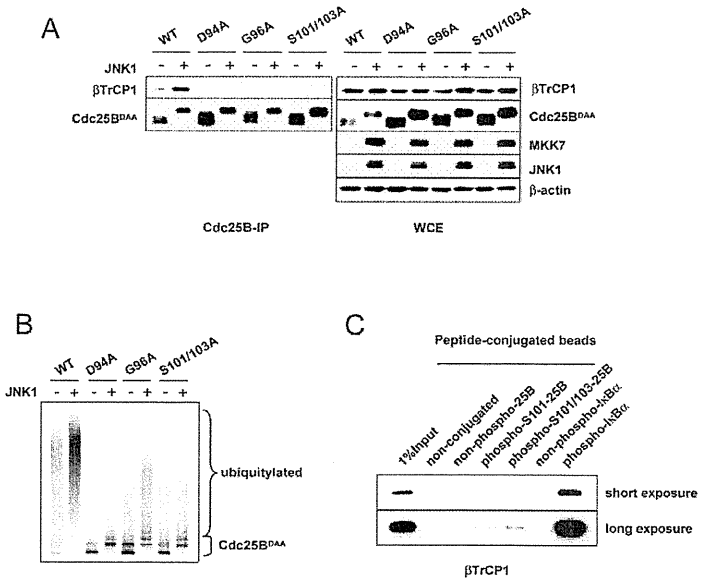

Fig. 5. Cdc25B peptide from D^{94}AG to S^{101}PSP is essential, but not sufficient, for Cdc25B ubiquitylation by SCF$^{\beta TrCP}$. (**A**) FLAG–Cdc25B of the wild type or indicated mutants was co-transfected with Myc–βTrCP1 in the presence or absence of JNK1. Then, 24 hours later, Cdc25B-bound βTrCP1 was detected by the immunoprecipitation of Cdc25B, followed by immunoblotting (Cdc25B-IP lanes). The expression of indicated proteins proteins is also shown (WCE lanes). (**B**) In vitro ubiquitylation by SCF$^{\beta TrCP1}$ of Cdc25B^{DAA} with wild-type DAG, or G96A or the double S101A, S103A mutations (S101/103A) was determined, as described in Fig. 2A. (**C**) Phosphorylated or unphosphorylated Cdc25B peptides, based on the sequence DAGLCMDSPSP that were conjugated with agarose beads, were incubated with Myc–βTrCP1-expressing Cos7 cell extracts and the βTrCP1 bound to peptides was detected by immunoblotting.

DAG was mutated to AAG (D94A), as the Asp in DSG plays a crucial role in substrate binding to βTrCP (Wu et al., 2003), and investigated whether the DAG in Cdc25B functions in JNK-induced βTrCP binding. FLAG–Cdc25B^{D94A} was co-transfected with βTrCP1 in the presence or absence of JNK1, and its binding to βTrCP1 was determined. Interestingly, Cdc25B^{D94A} failed to bind βTrCP1 (Fig. 4A). Cdc25B^{G96A} (DAA instead of DAG) was also unable to bind βTrCP1 (Fig. 4A). Furthermore, supplementary material Fig. S5A shows that both Cdc25B^{D94A} and Cdc25B^{G96A} were refractory to JNK-induced degradation (see also Fig. 1B). As expected, the Cdc25B S101A, S103A double mutant also lost βTrCP-binding ability. These results suggest that the Cdc25B peptide from D94 to S101 is a minimal requirement for βTrCP binding (see Fig. 1A). Moreover, the steady-state expression of such mutant Cdc25B was much higher than that of the wild-type protein (Fig. 5A). Therefore, the DAG sequence seems to be deeply involved in both the steady-state and stress-induced degradation of Cdc25B.

Next, we investigated how mutations in the DAG sequence affected in vitro Cdc25B ubiquitylation. Cdc25B^{D94A} was not ubiquitylated by SCF$^{\beta TrCP1}$, even in the presence of JNK activity; its ubiquitylation level was much less than that of the S101A, S103A double mutant (Fig. 5B). Cdc25B ubiquitylation was also greatly compromised by a G96A mutation, suggesting that G96 plays a role in Cdc25B binding to βTrCP. Cdc25B^{D94A} was phosphorylated at S101 and S103 when JNK1 was co-transfected (supplementary material Fig. S5B), showing that the phosphorylation of SPSP occurs irrespective of DAG. These results indicate that DAG in Cdc25B is necessary for ubiquitylation by SCF$^{\beta TrCP}$.

To elucidate whether a peptide encompassing DAG to SPSP was sufficient for βTrCP binding, we analysed βTrCP1 binding using the DAGLCMDSPSP peptide, in the unphosphorylated, S101-*P* and S101-*P*–P103-*P* forms. Peptide-conjugated beads were incubated with crude cell extracts prepared from βTrCP1-transfected Cos7 cells, and peptide-bound βTrCP1 was detected by immunoblotting. The unphosphorylated and phosphorylated IκBα peptides containing the conserved consensus βTrCP-binding sequence were used as controls. Fig. 5C shows that βTrCP1 barely bound the Cdc25B phospho-peptide under conditions where strong binding to the phosphorylated IκBα peptide was detected. Faint βTrCP1 signals that indicated binding to the doubly phosphorylated Cdc25B peptide were in fact detected by longer exposure. Taken together, these results strongly support the idea that DAG is a crucial sequence for JNK-induced Cdc25B ubiquitylation, but that the doubly phosphorylated DAGLCMDSPSP alone is insufficient for βTrCP binding.

The PEST-like sequence plays an important role in SCF$^{\beta TrCP}$-mediated Cdc25B ubiquitylation

Compared with Cdc25A, human Cdc25B possesses a longer PEST-like sequence that is rich in Glu (E) and Ser but lacks Pro (P), and is located upstream from DAG (Fig. 1A). This PEST-like sequence might contribute to βTrCP binding because phosphorylation or the presence of acidic amino acids N-terminal to the consensus DSG and DDG sequences facilitates βTrCP binding (Jin et al., 2003; Kanemori et al., 2005; Westbrook et al., 2008). The PEST-like sequence in Cdc25B comprises 12 amino acids, which consists of three ESS units and one LSS unit. We mutated all eight Ser to non-phosphorylatable Ala (S83A–S93A) and examined the binding of this sequence to βTrCP1. This Cdc25B^{8SA} mutant [denoted '8SA (–PEST)' in Fig. 5] was unable to bind βTrCP1 and was resistant to JNK-induced degradation (Fig. 6A and supplementary material Fig. S6A).

Next, we examined how many of the Cdc25B ESS–LSS sequences were necessary for βTrCP binding. We made a series of mutants with Ser-to-Ala mutations in the AA units, in which 2SA represents S83 and S84 to A, 4SA represents S83, S84, S86 and S87 to A, 6SA represents S86, S87, S89, S90, S92 and S93 to A, and 8SA is as described above (–PEST; see Fig. 6B) in the Cdc25^{DAA} background. The βTrCP-binding activity of these mutants was roughly proportional to the number of intact SS sequences (Fig. 6B). Consistent with these results, the degree of JNK-dependent ubiquitylation decreased in Cdc25B that lacked SS sequences (Fig. 6C). Cdc25B with fewer SS sequences was more refractory to JNK-induced degradation (supplementary

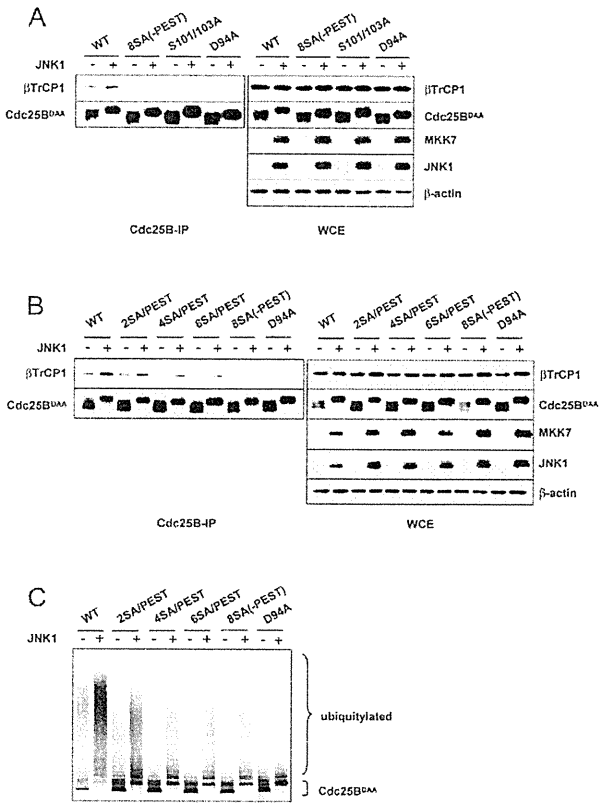

Fig. 6. The PEST-like sequence is required for efficient ubiquitylation of Cdc25B. (**A**) The following FLAG–Cdc25B^{DAA}-based mutants were co-transfected with Myc–βTrCP1 in the presence or absence of JNK1: WT with an intact PEST-like sequence; 8SA(–PEST) with mutations of eight Ser residues in the PEST-like sequence to alanine; the double S101A, S103A (S101/103A); or D94A. After 24 hours, Cdc25B was immunoprecipitated, and Cdc25B-bound βTrCP1 was detected by immunoblotting (Cdc25B-IP lanes). The expression of the indicated proteins was also determined (WCE lanes). (**B**) FLAG–Cdc25B^{DAA} with an intact PEST-like sequence (WT) or with SS to AA mutations of two Ser residues in three ESS units or one LSS unit was co-transfected with Myc–βTrCP1 in the presence or absence of JNK. The Cdc25B-bound βTrCP1 and protein expression are shown as indicated in A. Cdc25B^{D94A} was used as a negative control. (**C**) The ^{35}S-labelled Cdc25B^{DAA}-based proteins used in B were processed to detect in vitro ubiquitylation, as described in Fig. 2A.

material Fig. S6B). Of the four 2SA mutants (S83A and S84A, S86A and S87A, S89A and S90A, S92A and S93A), the mutant with SS mutations closest to DAG (S92A and S93A) was the most refractory to JNK-induced degradation and the least ubiquitylated, suggesting that ESS phosphorylation closer to DAG is more important for degradation (supplementary material Fig. S6C). The mutation in either E88 or E91 did not have any effect on JNK-induced degradation (supplementary material Fig. S6D), excluding the possibility that the PEST-like sequence itself is a core βTrCP-binding site. Moreover, S101 and S103 are phosphorylated in Cdc25B^{8SA}, indicating that the phosphorylation of S101 and S103 is independent of the PEST-like sequence (supplementary material Fig. S6E). Collectively, these results clearly indicate that a PEST-like sequence located upstream of DAG plays a crucial role in SCF^{βTrCP}-mediated Cdc25B ubiquitylation.

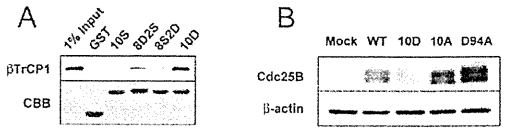

Fig. 7. A peptide encompassing the region between E^{82}SS and S^{101}PSP is a possible βTrCP-binding sequence in Cdc25B. (**A**) GST-fused Cdc25B-derived peptides consisting of the sequence E82SS to S101PSP were mixed with crude cell extracts prepared from Myc-tagged βTrCP1-transfected Cos7 cells, and this was followed by the recovery of proteins bound to GST-fused peptides. The recovered βTrCP1 was detected with anti-Myc antibody. The reaction mixture included 1 μM staurosporine to avoid the phosphorylation of Ser residues in the peptides by kinases present in the cell extracts. (**B**) FLAG–Cdc25B of wild type, 10D (all Ser residues in E^{82}SS to S^{101}PSP were replaced with Asp), 10A (all Ser residues in E^{82}SS to S^{101}PSP were replaced with Ala) or D94A were transfected into HeLa cells and their expression was determined by immunoblotting.

A stretch of PEST-like sequence up to S^{101}PSP of Cdc25B is a possible minimum sequence required for JNK-induced βTrCP binding

Next, we investigated the requirement of the PEST-like sequence and S^{101}PSP in βTrCP binding. Given the difficulty synthesising Ser-rich peptides and their phosphorylated forms, we made GST-fused peptides running from E^{82}SS to S^{101}PSP and their phospho-mimetic mutants, purified them from *Escherichia coli*, and investigated their binding to βTrCP1. The GST-fused peptides used were as follows: 10S (non-phosphorylated form), 8D2S (S-to-D mutation in the PEST-like sequence), 8S2D (D^{101}PDP mutant) and 10D (all S to D; Fig. 7A). Such *E. coli*-produced proteins were mixed with Myc–βTrCP1-expressing Cos7 cell extracts in the presence of 1 μM staurosporine to avoid phosphorylation of the GST-fused peptides by the kinases in Cos7 cell extracts. Peptide-bound βTrCP1 was detected by immunoblotting. As expected, the βTrCP1 bound to the phospho-mimetic peptides, but not the unphosphorylated one (Fig. 7A). βTrCP1 bound strongly to GST–10D, and less strongly to GST–8D2S and GST–8S2D. No βTrCP1 binding was detected for the GST-10S peptide. These results strongly suggest that the phosphorylation of Ser residues is required in the βTrCP-binding peptide consisting of the sequence from E^{82}SS to S^{101}PSP.

Next, we examined the stability of the Cdc25B^{10D} mutant in HeLa cells. Cdc25B of wild type, 10D, 10A (all Ser residues in E^{82}SS to S^{101}PSP were replaced by non-phosphorylatable Ala), and D94A were transfected to HeLa cells and their expression was detected in the absence of stress. As indicated in Fig. 7B, the expression of the phospho-mimetic Cdc25B^{10D} mutant was less than that of the wild type, indicating that Cdc25B^{10D} is unstable, even under unstressed conditions, supporting the idea that full βTrCP binding requires phosphorylation.

Finally, we investigated the contribution of the DAG and DDG βTrCP-binding sites to Cdc25B stability in stressed and unstressed conditions. FLAG–Cdc25B of wild type, Cdc25B^{D94A}, Cdc25B^{DAA} or Cdc25B$^{D94A/DAA}$ was transfected to HeLa cells and its expression was determined by immunoblotting. Typical expression of such mutants under anisomycin stress is shown in Fig. 8A. βTrCP1 binding to the Cdc25B mutant in the presence of JNK activity is also shown in supplementary material Fig. S7. As expected, Cdc25B^{WT} and Cdc25B^{DAA} were susceptible to anisomycin treatment and Cdc25B^{D94A} was more refractory to it. The

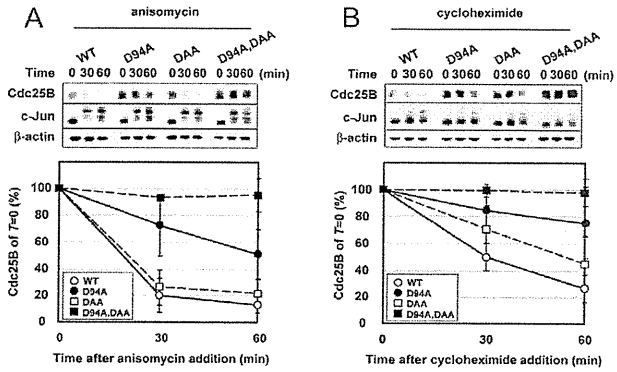

Fig. 8. DAG and DDG collaboratively regulate Cdc25B stability. FLAG-tagged Cdc25B^{WT}, Cdc25B^{D94A}, Cdc25B^{DAA} or Cdc25B$^{D94A/DAA}$ was transfected into HeLa cells, which were treated with 100 ng/ml anisomycin (**A**) or 50 μg/ml cycloheximide (**B**) 24 hours after transfection. Crude cell extracts were prepared at the indicated times and the expression of Cdc25B, Jun and β-actin was determined by immunoblotting. The relative expression of Cdc25B is also shown with the value at time 0 set to 100. The bars indicated the s.d. of five independent experiments. In A and B, the relative densitometric values of the expression of Cdc25B^{WT}, Cdc25B^{D94A}, Cdc25B^{DAA} and Cdc25B$^{D94A/DAA}$ were 1, 1.98±0.79, 1.77±0.59 and 4.21±1.2, respectively.

degradation of Cdc25B$^{D94A/DAA}$ was quite stable under anisomycin stress. These results indicate that the newly identified DAG βTrCP-binding sequence is responsible for stress-induced Cdc25B degradation. We also investigated the stability of such Cdc25B proteins in the presence of cycloheximide to estimate their steady-state stability (Fig. 8B). Cdc25B^{DAA} was more stable than Cdc25B^{WT}, but Cdc25B^{D94A} was even more stable than Cdc25B^{WT} or Cdc25B^{DAA}. Here again, the degradation of Cdc25B$^{D94A/DAA}$ was not observed with cycloheximide. These results suggest that the newly identified Cdc25B N-terminal βTrCP-binding region controls Cdc25B stability under both stressful and steady-state conditions and that the N-terminal DAG and constitutive DDG βTrCP binding sites cooperatively control Cdc25B stability.

Discussion

Previously, we showed that the cellular stresses that activate JNK or p38 induce Cdc25B degradation and that S101 and S103 are involved in Cdc25B stability (Uchida et al., 2009). We also suggested the involvement of the ubiquitin–proteasome system in stress-induced Cdc25B degradation. In this report, we identified SCF$^{\beta TrCP}$ as the ubiquitin ligase responsible for non-genotoxic stress-induced Cdc25B degradation. Moreover, S101 and S103 are highly phosphorylated by such stresses and are involved in ubiquitylation by SCF$^{\beta TrCP}$.

Our results indicate that non-canonical D^{94}AG and S^{101}PSP in Cdc25B play important roles in βTrCP binding. Moreover, an upstream PEST-like sequence starting from E^{82}SS turned out to have a crucial role in βTrCP binding to Cdc25B. Human Cdc25B has a longer PEST-like sequence than Cdc25A. The entire 12-amino-acid PEST-like sequence was essential for proper ubiquitylation. These results strongly indicate that the PEST-like sequence and SPSP cooperate with DAG for Cdc25B ubiquitylation under conditions that activate p38 and JNK. Moreover, the newly identified βTrCP-binding sequence around DAG is probably involved in Cdc25B degradation in collaboration with DDG under both stress-induced and steady-state conditions, given that the Cdc25B$^{D94A/DAA}$ double mutant was stable irrespective of cellular stress and SCF$^{\beta TrCP}$ barely ubiquitylated Cdc25B$^{D94A/DAA}$. Hence, we confidently conclude that Cdc25B stability is regulated mainly by SCF$^{\beta TrCP}$-mediated ubiquitylation via two independent sites: DAG and DAA.

The Ser residues in S^{101}PSP, located downstream from D94AG, are highly phosphorylated upon JNK and p38 activation. In addition, a GST-fused phospho-mimetic peptide consisting of E^{82}SS to S^{101}PSP bound βTrCP1, whereas that with the wild-type PEST-like sequence with SPSP did not, suggesting that the highly phosphorylated PEST-like sequence in Cdc25B is crucial for βTrCP binding. These results strongly suggest that full phosphorylation of the stretch from E^{82}SS to S^{101}PSP is required for Cdc25B to bind βTrCP. Such phosphorylation might confer a negative charge. The importance of phosphorylation in the upstream sequences to the core DSG sequence has also been reported in Cdc25A and REST (Jin et al., 2003; Westbrook et al., 2008). The stability of *Xenopus* Cdc25A was also found to be strongly affected by negatively charged amino acids surrounding the constitutive βTrCP-binding motif DDG (Kanemori et al., 2005). Hence, the βTrCP-binding-motif-like DAG sequence in Cdc25B functions in βTrCP binding by virtue of the strong negative charge resulting from acidic residues, which might enable a strong interaction with βTrCP. Analysis of the crystal structure should confirm this.

Under non-genotoxic stress, the Ser residues of the SPSP sequence are preferentially phosphorylated by p38 and JNK. Interestingly, S101 was weakly but constitutively phosphorylated under steady-state conditions when both p38 and JNK were inactive. These results indicate that an unidentified proline-directed kinase(s) phosphorylates S101 in the steady-state condition, which might contribute to Cdc25B degradation during the interphase. In this context, Isoda et al. reported the inhibition of phosphorylation by the CDK inhibitor p21 in the corresponding Ser residue in *Xenopus* Cdc25A (Isoda et al., 2009). Perhaps the interphase-specific CDK–cyclins that are active from the G1 phase to the S phase, such as Cdk2–cyclin E, Cdk2–cyclin A, and possibly Cdk4–cyclin D, phosphorylate S101 to keep Cdc25B expression low. The identification of a kinase that phosphorylates Cdc25B S101 under steady-state conditions is probably important for understanding the post-translational regulation of Cdc25B. A need for phosphorylation in the Cdc25B PEST-like sequence for βTrCP binding was also suggested. Given that the phosphorylation of Ser residues in the PEST-like sequence is a prerequisite for βTrCP binding, it is also important to identify the kinase(s) responsible for a full understanding of Cdc25B regulation. More work is needed to understand the regulation of Cdc25B stability by phosphorylation under steady-state and stress-induced conditions.

In conclusion, we identified a new site in Cdc25B for non-genotoxic stress-induced βTrCP binding and proved that SCF$^{\beta TrCP}$ is the responsible ubiquitin ligase. The newly identified site is DAG, which is thought to be inactive in βTrCP binding; it is surrounded by an upstream PEST-like sequence and a downstream SPSP. Our results suggest that the full phosphorylation of the PEST-like sequence and SPSP are required for βTrCP binding and that the new site and the previously reported DDG constitutive βTrCP binding site collaboratively regulate the stability of Cdc25B under both stress-induced and steady-state conditions. Cdc25B and Cdc25A are overexpressed in many tumours, and their overexpression is correlated with a poor prognosis (Kristjansdottir and Rudolph, 2004; Boutros et al., 2007). The uncontrolled

expression of Cdc25B is itself toxic, as it induces premature entry into M phase (Karlsson et al., 1999) and possibly genomic instability. Further studies that elucidate the regulation of Cdc25B stability should increase our understanding of the role of Cdc25B in cell cycle control and the contribution of the deregulation of Cdc25B stability to tumorigenesis.

Materials and Methods

Reagents and plasmids

Reagents of the highest grade were obtained from Wako (Osaka, Japan) or Sigma. The following siRNAs were purchased from Dharmacon: βTrCP1–βTrCP2 [denoted as pan-βTrCP siRNA in reports by Margottin-Goguet et al. and Guardavaccaro et al. (Margottin-Goguet et al., 2003; Guardavaccaro et al., 2003)], βTrCP1 (5′-UGACAA-CACUAUCAGAUUA-3′), and βTrCP2 (5′-GGACUUUAUUACCGCUUUA-3′). The validated stealth RNAi for JNK1 (5′-GGGCCUACAGAGAGCTAGUUCU-UAU-3′) and JNK2 (5′-GCCCAAGGGAUUGUUUGUGCUGCAU-3′ and 5′-GC-CAACUGUGAGGAAUUAUGUCGAA-3′) were obtained from Invitrogen. The siRNA for luciferase (5′-CGUACGCGGAAUACUUCGA-3′) was obtained from Qiagen. Anisomycin, SB202190, PD169316 and SP600125 were obtained from Calbiochem. The following cDNAs were used: human Cdc25B1, human Cdc25B3, mouse Cdc25B1, mouse p38α, mouse MKK6, mouse JNK1, mouse MKK7, human βTrCP1, human βTrCP2, human Skp1, human Skp2, human Cdc4, human Cul1 and mouse Rbx1. FLAG-, HA- and Myc-tagged expression plasmids were constructed using the pEF6/Myc-His vector, which includes the EF1α promoter (Invitrogen), as described elsewhere (Uchida et al., 2004). The mutant versions of the above cDNAs were generated by PCR-based mutagenesis, and their nucleotide sequences were confirmed by sequencing.

Antibodies and proteins

Active JNK1 kinase was purchased from Invitrogen. The rabbit antibody specific for Cdc25B S101-*P* was obtained from GenScript Corporation using NH_2-MD-*P*SPSPMDPHMAEC-COOH as the antigen. The rabbit antibodies specific for S103-*P*, and S101-*P* and S103-*P* were obtained from IBL (Japan) using NH_2-MDSP-*P*SPMDPHMAEC-COOH and NH_2-MD-*P*SP-*P*SPMDPHMAEC-COOH as the respective antigens. Each anti-phosphorylated antibody was affinity purified with antigen peptide before use. The antibodies purchased were as follows: mouse anti-TrCP1 was purchased from Zymed; Cdc25A (F-6), Cdc25B (C-20) and JNK1 (C-17) antibodies were from Santa Cruz Biotechnology; anti-actin, Myc tag (9B11), HA tag 262K, phosphoylated JNK–T183/Y185 (G9), MK2, Jun and phosphorylated Jun-S63II were obtained from Cell Signaling. The anti-Cdc25B (AF1649) was obtained from R&D Systems. Secondary antibodies labelled with horseradish peroxidase were purchased from DAKO. Anti-FLAG–M2-agarose beads were purchased from Sigma. The rabbit anti-FLAG serum was raised in-house. *E. coli*-produced GST-fused Cdc25B peptides encompassing $E^{82}SS$ to $S^{101}PSP$ and the phospho-mimetic mutant versions were purified from IPTG-induced BL21 cells with glutathione beads (GE Healthcare).

Cells, cell culture and siRNA or plasmid transfection

HeLa and Cos7 cells were grown in Dulbecco's modified Eagle's medium (DMEM) containing high glucose (Sigma) supplemented with 10% foetal bovine serum (FBS; Hyclone) and antibiotics. HeLa-W40 cells that constitutively expressed FLAG-tagged wild-type Cdc25B under the EF1α promoter were also cultured under the same conditions (Uchida et al., 2009). We also isolated HeLa cells constitutively expressing the FLAG-tagged $Cdc25B^{DAA}$ mutant (HeLa-DAA34 cells). In these cells, the expression of external Cdc25B was roughly 20- to 40-fold higher than that of endogenous Cdc25B. Plasmids were transiently transfected with Lipofectamine 2000 (Invitrogen). The amount of plasmid DNA used for transfection was ~500 ng for a six-well plate. HeLa and Cos7 cells were used for assays of stability (degradation) and for protein–protein interaction, respectively. The siRNA was transfected using Lipofectamine RNAiMAX (Invitrogen).

Biochemical methods and in vitro ubiquitylation assay

Crude extraction of proteins for analysis followed by immunoblotting or immunoprecipitation was performed as described previously (Uchida et al., 2004). The in vitro ubiquitylation assay was performed essentially as described previously (Watanabe et al., 2004). Briefly, HA-tagged Rbx1, Skp2 and Cul1, and Myc-tagged F-box proteins were coexpressed in Cos7 cells, and the SCF complex was recovered by immunoprecipitation with anti-Myc–agarose (MBL, Japan). [^{35}S]methionine-labelled Cdc25B was prepared with a TNT-coupled transcription and translation system (Promega). The reaction mixture in a total volume of 20 μl contained SCF-complex on beads, ^{35}S-labelled Cdc25B (2 μl), 20 μg bovine ubiquitin (Sigma), 0.8 μg human recombinant E1 enzyme (BIOMOL), 1 μg human 6xHis–Ubc5 (Wako, Osaka, Japan) and an ATP-regenerating system (2 mM ATP, 10 mM creatine phosphate, 0.35 IU/ml creatine kinase, 0.6 IU/ml inorganic pyrophosphatase), supplemented with 5 μM MG132, 0.5 μM okadaic acid and 1 μM ubiquitin-aldehyde (Boston Biochem). When necessary, recombinant active JNK1 (25 ng) was added to the reaction. The mixtures were incubated at 37°C for 2 hours, followed by sodium dodecyl sulphate–polyacrylamide gel electrophoresis (SDS-PAGE) in a 2–15% gradient gel, and the ubiquitylated Cdc25B was visualised using the FUJI BAS system.

We thank S. I. Reed (Scripps Institute) for the generous gift of human Cdc4 plasmids. This work was supported by grants from the following institutions: The Ministry of Health, Labour and Welfare of Japan, the Ministry of Culture, Sports, Science and Technology of Japan, the Research Grants Council of Hong Kong, the Cosmetology Research Foundation, the Long-range Research Initiative (LRI) of the Japan Chemical Industry Association, and the Japan Science and Technology Agency.

Supplementary material available online at
http://jcs.biologists.org/cgi/content/full/124/15/2816/DC1

References

Baldin, V., Cans, C., Superti-Furga, G. and Ducommun, B. (1997). Alternative splicing of the human CDC25B tyrosine phosphatase. Possible implications for growth control? *Oncogene* **14**, 2485-2495.

Bartek, J., Lukas, C. and Lukas, J. (2004). Checking on DNA damage in S phase. *Nat. Rev. Mol. Cell Biol.* **5**, 792-804.

Boutros, R., Dozier, C. and Ducommun, B. (2006). The when and wheres of CDC25 phosphatases. *Curr. Opin. Cell Biol.* **18**, 185-191.

Boutros, R., Lobjois, V. and Ducommun, B. (2007). CDC25 phosphatases in cancer cells: key players? Good targets? *Nat. Rev. Cancer* **7**, 495-507.

Busino, L., Donzelli, M., Chiesa, M., Guardavaccaro, D., Ganoth, D., Dorrello, N. V., Hershko, A., Pagano, M. and Draetta, G. F. (2003). Degradation of Cdc25A by beta-TrCP during S phase and in response to DNA damage. *Nature* **426**, 87-91.

Busino, L., Chiesa, M., Draetta, G. F. and Donzelli, M. (2004). Cdc25A phosphatase: combinatorial phosphorylation, ubiquitylation and proteolysis. *Oncogene* **23**, 2050-2056.

Chen, M. S., Hurov, J., White, L. S., Woodford-Thomas, T. and Piwnica-Worms, H. (2001). Absence of apparent phenotype in mice lacking Cdc25C protein phosphatase. *Mol. Cell. Biol.* **21**, 3853-3861.

Donzelli, M. and Draetta, G. F. (2003). Regulating mammalian checkpoints through Cdc25 inactivation. *EMBO Rep.* **4**, 671-677.

Ferguson, A. M., White, L. S., Donovan, P. J. and Piwnica-Worms, H. (2005). Normal cell cycle and checkpoint responses in mice and cells lacking Cdc25B and Cdc25C protein phosphatases. *Mol. Cell. Biol.* **25**, 2853-2860.

Frescas, D. and Pagano, M. (2008). Deregulated proteolysis by the F-box proteins SKP2 and beta-TrCP: tipping the scales of cancer. *Nat. Rev. Cancer* **8**, 438-449.

Galaktionov, K., Lee, A. K., Eckstein, J., Draetta, G., Meckler, J., Loda, M. and Beach, D. (1995). CDC25 phosphatases as potential human oncogenes. *Science* **269**, 1575-1577.

Guardavaccaro, D., Kudo, Y., Boulaire, J., Barchi, M., Busino, L., Donzelli, M., Margottin-Goguet, F., Jackson, P. K., Yamasaki, L. and Pagano, M. (2003). Control of meiotic and mitotic progression by the F box protein beta-Trcp1 *in vivo*. *Dev. Cell* **4**, 799-812.

Isoda, M., Kanemori, Y., Nakajo, N., Uchida, S., Yamashita, K., Ueno, H. and Sagata, N. (2009). The extracellular signal-regulated kinase-mitogen-activated protein kinase pathway phosphorylates and targets Cdc25A for $SCF^{beta\text{-}TrCP}$-dependent degradation for cell cycle arrest. *Mol. Biol. Cell* **20**, 2186-2195.

Jin, J., Shirogane, T., Xu, L., Nalepa, G., Qin, J., Elledge, S. J. and Harper, J. W. (2003). $SCF^{beta\text{-}TrCP}$ links Chk1 signaling to degradation of the Cdc25A protein phosphatase. *Genes Dev.* **17**, 3062-3074.

Kakizuka, A., Sebastian, B., Borgmeyer, U., Hermans-Borgmeyer, I., Bolado, J., Hunter, T., Hoekstra, M. F. and Evans, R. M. (1992). A mouse cdc25 homolog is differentially and developmentally expressed. *Genes Dev.* **6**, 578-590.

Kanemori, Y., Uto, K. and Sagata, N. (2005). Beta-TrCP recognizes a previously undescribed nonphosphorylated destruction motif in Cdc25A and Cdc25B phosphatases. *Proc. Natl. Acad. Sci. USA* **102**, 6279-6284.

Karlsson, C., Katich, S., Hagting, A., Hoffmann, I. and Pines, J. (1999). Cdc25B and Cdc25C differ markedly in their properties as initiators of mitosis. *J. Cell Biol.* **146**, 573-584.

Kristjansdottir, K. and Rudolph, J. (2004). Cdc25 phosphatases and cancer. *Chem. Biol.* **11**, 1043-1051.

Latres, E., Chiaur, D. S. and Pagano, M. (1999). The human F box protein beta-TrCP associates with the Cul1/Skp1 complex and regulates the stability of beta-catenin. *Oncogene* **18**, 849-854.

Lee, G., White, L. S., Hurov, K. E., Stappenbeck, T. S. and Piwnica-Worms, H. (2009). Response of small intestinal epithelial cells to acute disruption of cell division through CDC25 deletion. *Proc. Natl. Acad. Sci. USA* **106**, 4701-4706.

Lincoln, A. J., Wickramasinghe, D., Stein, P., Schultz, R. M., Palko, M. E., De Miguel, M. P., Tessarollo, L. and Donovan, P. J. (2002). Cdc25b phosphatase is required for resumption of meiosis during oocyte maturation. *Nat. Genet.* **30**, 446-449.

Ma, Z. Q., Chua, S. S., DeMayo, F. J. and Tsai, S. Y. (1999). Induction of mammary gland hyperplasia in transgenic mice over-expressing human Cdc25B. *Oncogene* **18**, 4564-4576.

Margottin-Goguet, F., Hsu, J. Y., Loktev, A., Hsieh, H. M., Reimann, J. D. and Jackson, P. K. (2003). Prophase destruction of Emi1 by the $SCF^{betaTrCP/Slimb}$ ubiquitin

ligase activates the anaphase promoting complex to allow progression beyond prometaphase. *Dev. Cell* **4**, 813-826.

Melixetian, M., Klein, D. K., Sorensen, C. S. and Helin, K. (2009). NEK11 regulates CDC25A degradation and the IR-induced G2/M checkpoint. *Nat. Cell Biol.* **11**, 1247-1253.

Miyata, H., Doki, Y., Yamamoto, H., Kishi, K., Takemoto, H., Fujiwara, Y., Yasuda, T., Yano, M., Inoue, M., Shiozaki, H. et al. (2001). Overexpression of CDC25B overrides radiation-induced G2-M arrest and results in increased apoptosis in esophageal cancer cells. *Cancer Res.* **61**, 3188-3193.

Morgan, D. O. (1995). Principles of CDK regulation. *Nature* **374**, 131-134.

Ray, D., Terao, Y., Nimbalkar, D., Hirai, H., Osmundson, E. C., Zou, X., Franks, R., Christov, K. and Kiyokawa, H. (2007). Hemizygous disruption of Cdc25A inhibits cellular transformation and mammary tumorigenesis in mice. *Cancer Res.* **67**, 6605-6611.

Seki, A., Coppinger, J. A., Du, H., Jang, C. Y., Yates, J. R., 3rd and Fang, G. (2008). Plk1- and beta-TrCP-dependent degradation of Bora controls mitotic progression. *J. Cell Biol.* **181**, 65-78.

Uchida, S., Kuma, A., Ohtsubo, M., Shimura, M., Hirata, M., Nakagama, H., Matsunaga, T., Ishizaka, Y. and Yamashita, K. (2004). Binding of 14-3-3beta but not 14-3-3sigma controls the cytoplasmic localization of CDC25B: binding site preferences of 14-3-3 subtypes and the subcellular localization of CDC25B. *J. Cell Sci.* **117**, 3011-3020.

Uchida, S., Yoshioka, K., Kizu, R., Nakagama, H., Matsunaga, T., Ishizaka, Y., Poon, R. Y. and Yamashita, K. (2009). Stress-activated mitogen-activated protein kinases c-Jun NH2-terminal kinase and p38 target Cdc25B for degradation. *Cancer Res.* **69**, 6438-6444.

Watanabe, N., Arai, H., Nishihara, Y., Taniguchi, M., Hunter, T. and Osada, H. (2004). M-phase kinases induce phospho-dependent ubiquitination of somatic Wee1 by SCF$^{beta\text{-}TrCP}$. *Proc. Natl. Acad. Sci. USA* **101**, 4419-4424.

Westbrook, T. F., Hu, G., Ang, X. L., Mulligan, P., Pavlova, N. N., Liang, A., Leng, Y., Maehr, R., Shi, Y., Harper, J. W. et al. (2008). SCF$^{beta\text{-}TrCP}$ controls oncogenic transformation and neural differentiation through REST degradation. *Nature* **452**, 370-374.

Winston, J. T., Strack, P., Beer-Romero, P., Chu, C. Y., Elledge, S. J. and Harper, J. W. (1999). The SCF$^{beta\text{-}TrCP}$-ubiquitin ligase complex associates specifically with phosphorylated destruction motifs in IκBα and β-catenin and stimulates IκBα ubiquitination *in vitro*. *Genes Dev.* **13**, 270-283.

Wu, G., Xu, G., Schulman, B. A., Jeffrey, P. D., Harper, J. W. and Pavletich, N. P. (2003). Structure of a beta-TrCP1-Skp1-beta-catenin complex: destruction motif binding and lysine specificity of the SCF$^{beta\text{-}TrCP1}$ ubiquitin ligase. *Mol. Cell* **11**, 1445-1456.

Yao, Y., Slosberg, E. D., Wang, L., Hibshoosh, H., Zhang, Y. J., Xing, W. Q., Santella, R. M. and Weinstein, I. B. (1999). Increased susceptibility to carcinogen-induced mammary tumors in MMTV-Cdc25B transgenic mice. *Oncogene* **18**, 5159-5166.

$SCF^{\beta TrCP}$ mediates stress-activated MAPK-induced Cdc25B degradation

JCS083931 Supplementary Material

Files in this Data Supplement:

- **Supplemental Figure S1 - Fig. S1. SCFβTrCP ubiquitylates Cdc25B.** (A) 35S-methione-labelled Cdc25BDAA of human B1, human B3, and mouse B1 was incubated with the SCFβTrCP complex in the presence or absence of JNK1, and the ubiquitylation was determined as described in the *Materials and Methods*. The ubiquitylation of 35S-methione-labelled Cdc25B1DAA with additional mutations of D94A or S101/103A was also determined. (B) The following FLAG-Cdc25BDAA-based mutants were cotransfected with Myc-βTrCP1 in the presence or absence of JNK1: WT without other mutation; S101A; S103A; S101/103A; or D94A. Then, 24 h later, Cdc25B-bound βTrCP1 was detected by the immunoprecipitation of Cdc25B, followed by immunoblotting (Cdc25B-IP panel). The expression of the indicated proteins is also shown (WCE panel).
- **Supplemental Figure S2 - Fig. S2. The depletion of βTrCP1/2 with siRNA stabilises Cdc25B.** (A) HeLa cells constitutively expressing FLAG-Cdc25B (HeLa-W40 cells) were transfected with control siRNA (against luciferase (Luci)) or siRNA that targets both βTrCP1 and βTrCP2 (βTrCP). After 24 h, the expression of FLAG-Cdc25B, endogenous Cdc25A, βTrCP1, and β-actin was determined by immunoblotting. (B) HeLa cells were transfected with siRNA against luciferase (Luci) or βTrCP (pan-βTrCP or βTrCP1 + 2). After 24 h, these cells were further transfected with FLAG-Cdc25BDAA with or without JNK1 and MKK7. After 24 h, the expression of Cdc25BDAA and the indicated proteins was determined by immunoblotting. (C) HeLa-DAA34 cells expressing FLAG-Cdc25BDAA were transfected with siRNA against either Luci or pan-βTrCP and challenged with 50 ng/mL anisomycin. The expression of the indicated proteins was determined by immunoblotting at the indicated time points. Quantitative results for the expression of

Cdc25BDAA are shown. The results shown are the average of three independent experiments with the SD.

- **Supplemental Figure S3 - Fig. S3. Cdc25B S101 and S103 are phosphorylated by JNK or by UV irradiation**. (A) The specificity of phospho-specific antibodies was evaluated using *in vitro* phosphorylated Cdc25B. The GST-fused Cdc25B N-terminal fragment (1−175) purified from *E. coli* was phosphorylated by JNK1 and probed with the indicated antibodies. (B) HeLa-W40 cells were irradiated with UV at 20 J/m2, and cell extracts were prepared at the indicated times. After the immunoprecipitation of Cdc25B with anti-FLAG beads, the phosphorylation status of the indicated amino acids was determined by immunoblotting with each phospho-specific antibody. The expression of the indicated proteins is also shown.
- **Supplemental Figure S4 - Fig. S4. p38 and JNK are involved in phosphorylation at S101 and S103**. HeLa-W40 cells were treated with the p38 inhibitor SB202190 (A), p38 inhibitor PD169316 (B), or JNK inhibitor SP600125 (C) at the indicated concentration 1 h before the challenge with 50 ng/mL anisomycin. FLAG-Cdc25B was recovered with anti-FLAG agarose beads, and then the expression and phosphorylation of S101 or S103 was determined by immunoblotting with specific antibodies. The expression of other proteins was also determined. (D) HeLa cells were transfected with the wild-type or kinase-dead form of JNK1 with MKK7. After 24 h, the expression of endogenous Cdc25B was determined by immunoprecipitation followed by immunoblotting. The expression of the indicated proteins is also shown. The transfection efficiency of JNK1 was about 75% (range 70−80%).
- **Supplemental Figure S5 - Fig. S5. Cdc25B DAG mutations stabilise Cdc25B**. (A) FLAG-Cdc25B of the wild type or D94A, G96A, or S101/103A mutants was cotransfected with or without JNK1. The expression of the indicated proteins was determined 24 h after transfection by immunoblotting. (B) Cdc25B of the wild type, D94A, or S101/103A was cotransfected with or without JNK1. After 24 h, cell extracts were prepared, and Cdc25B was immunoprecipitated with

anti-FLAG beads, followed by the determination of Cdc25B S101/103 phosphorylation by immunoblotting.

- **Supplemental Figure S6 - Fig. S6. The Cdc25B PEST-like sequence plays an important role in JNK-induced degradation**. (A) FLAG-Cdc25B of the wild-type or PEST-like sequence mutant (all eight serine residues in the PEST-like sequence were mutated to alanine, 8SA -PEST), S101/103A, or D94A mutants were transfected into HeLa cells in the presence or absence of JNK1. The expression of the indicated proteins was determined 24 h after transfection. (B) FLAG-Cdc25B of the wild-type or PEST-like sequence mutants in which different numbers of serine residues were mutated to alanine were transfected to HeLa cells with or without JNK1. The expression of the indicated proteins was determined 24 h after transfection. (C) FLAG-Cdc25B mutants with mutations in two serine residues in each ESS unit or in LSS in the PEST-like sequence were transfected with or without JNK1. The expression of the indicated proteins was determined 24 h after transfection. (D) FLAG-Cdc25B of wild type or the E88A, E91A, or D94A mutant was transfected with or without JNK1. The expression of the indicated proteins was determined 24 h after transfection. (E) Cdc25B of the wild type, 8SA (-PEST), S101/103A, or D94A was cotransfected with or without JNK1. After 24 h, cell extracts were prepared, and Cdc25B was immunoprecipitated with anti-FLAG beads, followed by the determination of Cdc25B S101/103 phosphorylation by immunoblotting.

Supplemental Figure S7 - Fig. S7. DAG is a JNK-dependent βTrCP1 site in Cdc25B and DDG is a JNK-independent site. FLAG-Cdc25B of the wild type or D94A, DAA, or D94A/DAA mutants was transfected with or without JNK1. After 24 h, the FLAG-Cdc25B proteins were recovered by immunoprecipitation and the βTrCP1 bound to FLAG-Cdc25B or recovered FLAG-Cdc25B was determined by immunoblotting (Cdc25B-IP). The expression of the indicated proteins 24 h after transfection is also shown (WCE).